
Figures and figure supplements

A mammalian *Wnt5a–Ror2–Vangl2* axis controls the cytoskeleton and confers cellular properties required for alveologenesis

Kuan Zhang et al

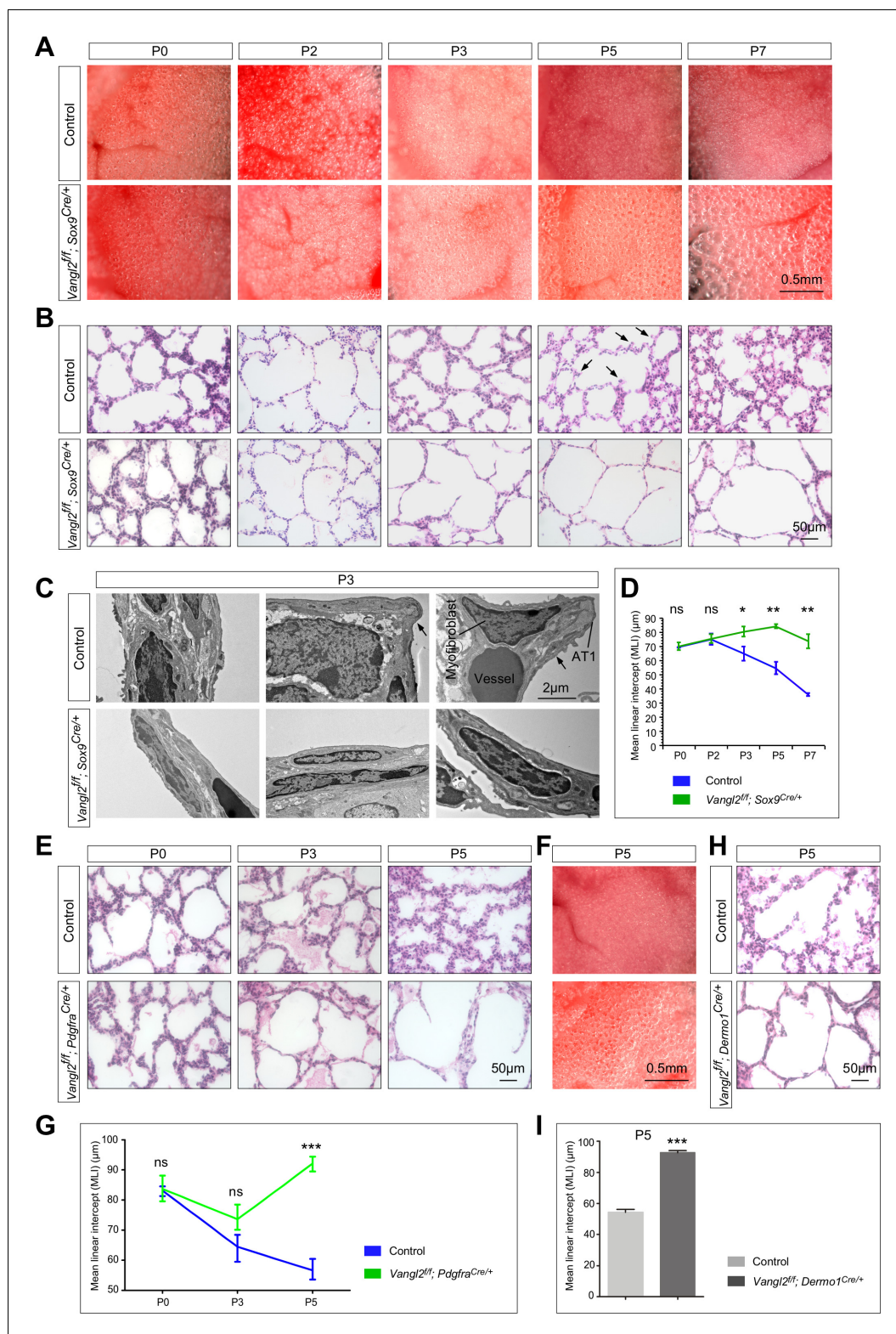


Figure 1. *Vangl2* is required in both the lung epithelium and mesenchyme for alveolar formation. (A) Surface view of dissected lungs from wild-type and *Vangl2^{fl/fl}; Sox9^{Cre/+}* mice at different postnatal (P) stages as indicated. Enlarged saccules were discerned in *Vangl2^{fl/fl}; Sox9^{Cre/+}* lungs at P3 and their size increased significantly as postnatal lung development proceeded. (B) Hematoxylin and eosin-stained lung sections of wild-type and *Vangl2^{fl/fl}; Sox9^{Cre/+}* mice at different postnatal stages. Histological analysis confirmed the presence of enlarged saccules in *Vangl2^{fl/fl}; Sox9^{Cre/+}* lungs. (C) Higher magnification histological images of lung sections at P3, showing myofibroblasts, vessels, and alveolar thickening (AT1) in *Vangl2^{fl/fl}; Sox9^{Cre/+}* mice. (D) Line graph showing mean linear intercept (MLI) in micrometers for Control (blue) and *Vangl2^{fl/fl}; Sox9^{Cre/+}* (green) mice from P0 to P7. MLI is significantly lower in the mutant group from P3 onwards. (E) Histological images of lung sections at P0, P3, and P5 for Control and *Vangl2^{fl/fl}; Pdgfra^{Cre/+}* mice. (F) Surface view of lungs at P5 for Control and *Vangl2^{fl/fl}; Dermo1^{Cre/+}* mice. (G) Line graph showing MLI for Control (blue) and *Vangl2^{fl/fl}; Pdgfra^{Cre/+}* (green) mice at P0, P3, and P5. MLI is significantly lower in the mutant group at P5. (H) Histological images of lung sections at P5 for Control and *Vangl2^{fl/fl}; Dermo1^{Cre/+}* mice. (I) Bar graph showing MLI at P5 for Control (grey) and *Vangl2^{fl/fl}; Dermo1^{Cre/+}* (black) mice. MLI is significantly lower in the mutant group.

Figure 1 continued on next page

Figure 1 continued

sacculi in *Vangl2*-deficient lungs starting at P3. Arrows point to rudimentary secondary septa. (C) Transmission electron micrographs of lungs from wild-type and *Vangl2*^{fl/fl}; *Sox9*^{Cre/+} mice at P3. Rudimentary secondary septa (arrows), in which the alveolar type I (AT1) cells encased myofibroblasts and blood vessels, were seen in control but not *Vangl2*-deficient lungs. (D) Measurement of the mean linear intercept (MLI) in wild-type and *Vangl2*^{fl/fl}; *Sox9*^{Cre/+} lungs (n = 3 for each group). The MLI was increased in *Vangl2*-deficient lungs, starting at P3. (E) Hematoxylin and eosin-stained lung sections of wild-type and *Vangl2*^{fl/fl}; *Pdgfra*^{Cre/+} mice at different postnatal stages. Enlarged sacculi were detected in *Vangl2*^{fl/fl}; *Pdgfra*^{Cre/+} lungs at P3 and their size increased significantly as postnatal lung development proceeded. (F) Surface view of dissected lungs from wild-type and *Vangl2*^{fl/fl}; *Pdgfra*^{Cre/+} mice at P5. Larger sacculi were found in *Vangl2* mutant lungs induced by *Pdgfra*^{Cre}. (G) Measurement of the MLI in wild-type and *Vangl2*^{fl/fl}; *Pdgfra*^{Cre/+} lungs (n = 3 for each group). The MLI was increased in *Vangl2*-deficient lungs, starting at P5. (H) Hematoxylin and eosin-stained lung sections of wild-type and *Vangl2*^{fl/fl}; *Dermo1*^{Cre/+} mice at P5. Larger sacculi were found in *Vangl2* mutant lungs induced by *Dermo1*^{Cre}. (I) Measurement of the MLI in wild-type and *Vangl2*^{fl/fl}; *Dermo1*^{Cre/+} lungs (n = 3 for each group). The MLI was increased in *Vangl2*-deficient lungs. All values are mean ± SEM. (*) p<0.05; (**) p<0.01; ns, not significant (unpaired Student's t-test).

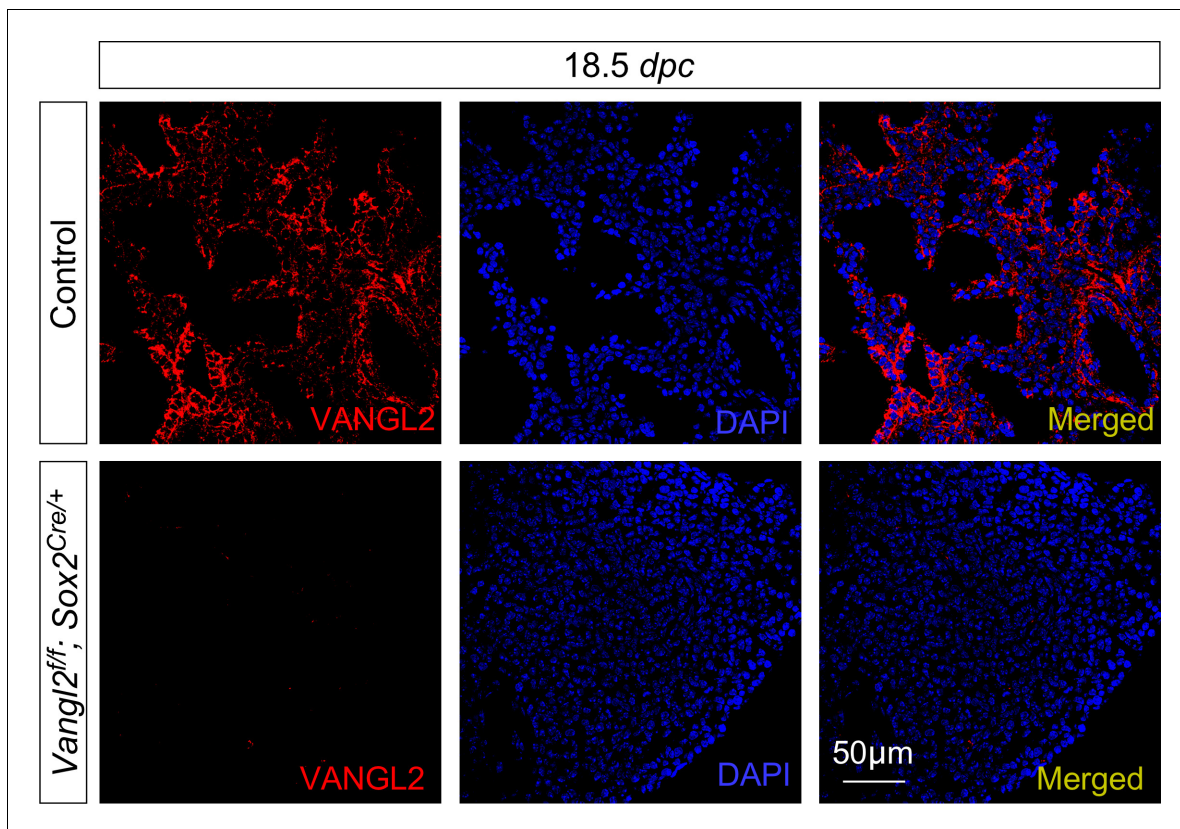


Figure 1—figure supplement 1. VANGL2 is broadly expressed in both the lung epithelium and mesenchyme. Immunostaining of lung sections collected from control and *Vangl2^{fl/fl}; Sox2^{Cre/+}* mice at 18.5 days post coitus (dpc). VANGL2 was detected in both the lung epithelium and mesenchyme in wild-type lungs. VANGL2 immunoreactivity was completely absent in the lungs of *Vangl2^{fl/fl}; Sox2^{Cre/+}* mice, validating the VANGL2 immunoreactivity detected by VANGL2 antibodies. Note that early expression of Sox2-Cre in all epiblast cells by 6.5 dpc effectively converted *Vangl2^f* into a null allele in all embryonic lineages. *Vangl2^{fl/fl}; Sox2^{Cre/+}* is in essence equivalent to *Vangl2^{-/-}*.

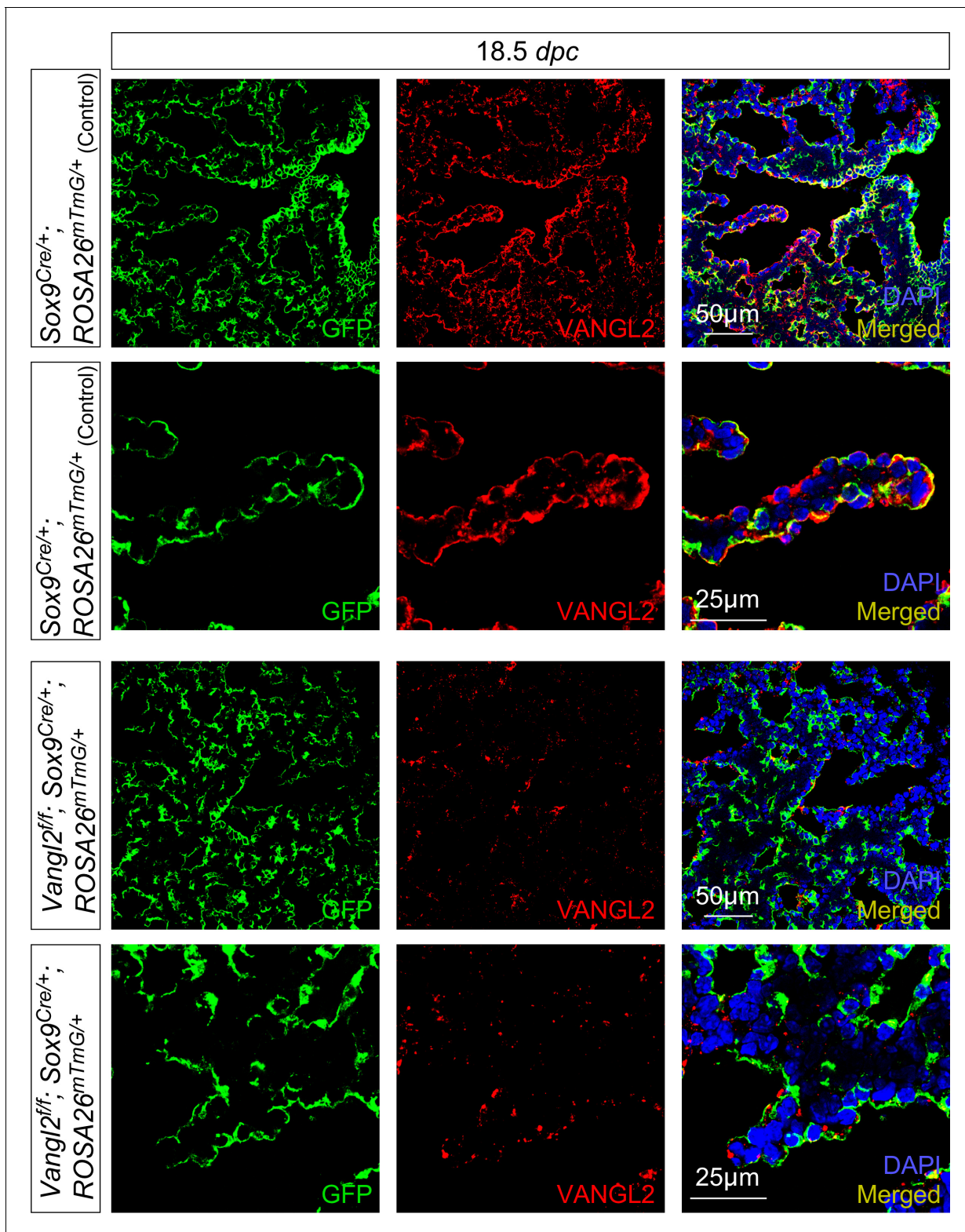


Figure 1—figure supplement 2. VANGL2 is selectively removed in the distal lung epithelium by Sox9-Cre. Immunostaining of lung sections collected from *Sox9^{Cre/+}; ROSA26^{mTmG/+}* (control) and *Vangl2^{ff}; Sox9^{Cre/+}; ROSA26^{mTmG/+}* mice at 18.5 days post coitus (dpc). Sox9-Cre induced GFP expression from the *ROSA26^{mTmG}* locus. VANGL2 immunoreactivity was selectively lost in the lung epithelium (GFP⁺) of *Vangl2^{ff}; Sox9^{Cre/+}; ROSA26^{mTmG/+}* mice; VANGL2 expression was retained in the lung mesenchyme.

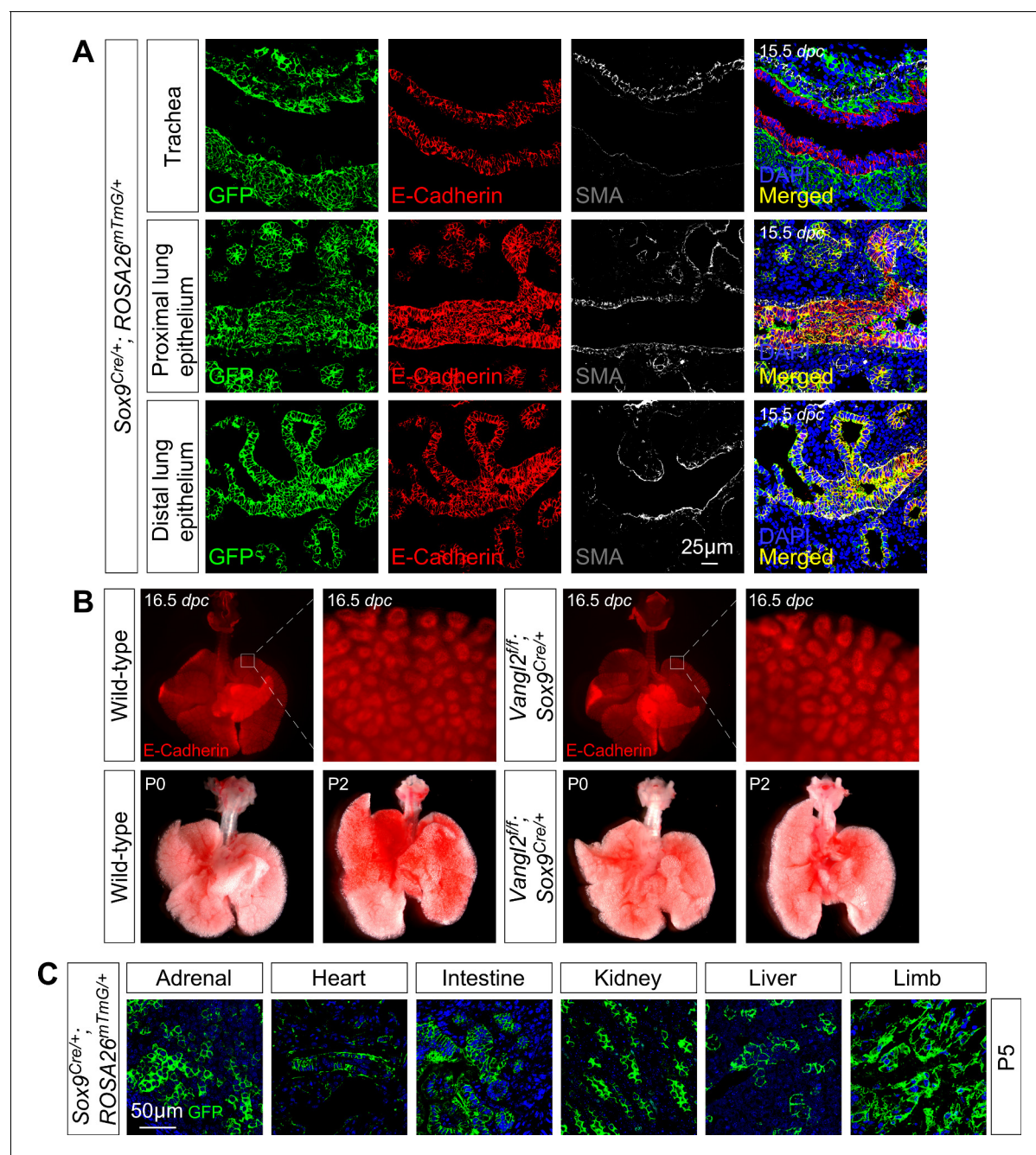


Figure 1—figure supplement 3. *Sox9-Cre* is broadly expressed but *Vangl2^{fl/fl}; Sox9^{Cre/+}* mice do not display defects in lung branching or sacculle formation. (A) Immunostaining of lung sections collected from *Sox9^{Cre/+}; ROSA26^{mTmG/+}* mice at 15.5 days post coitus (dpc). (B) Ventral views of dissected lungs from control or *Vangl2^{fl/fl}; Sox9^{Cre/+}* mice at 16.5 dpc, postnatal (P) day 0 or 2. No apparent phenotypes in branching (likely due to the presence of *Vangl1*) or sacculcation were discerned in the mutant lungs. (C) Immunostaining of sections of various tissues collected from *Sox9^{Cre/+}; ROSA26^{mTmG/+}* mice at P5.

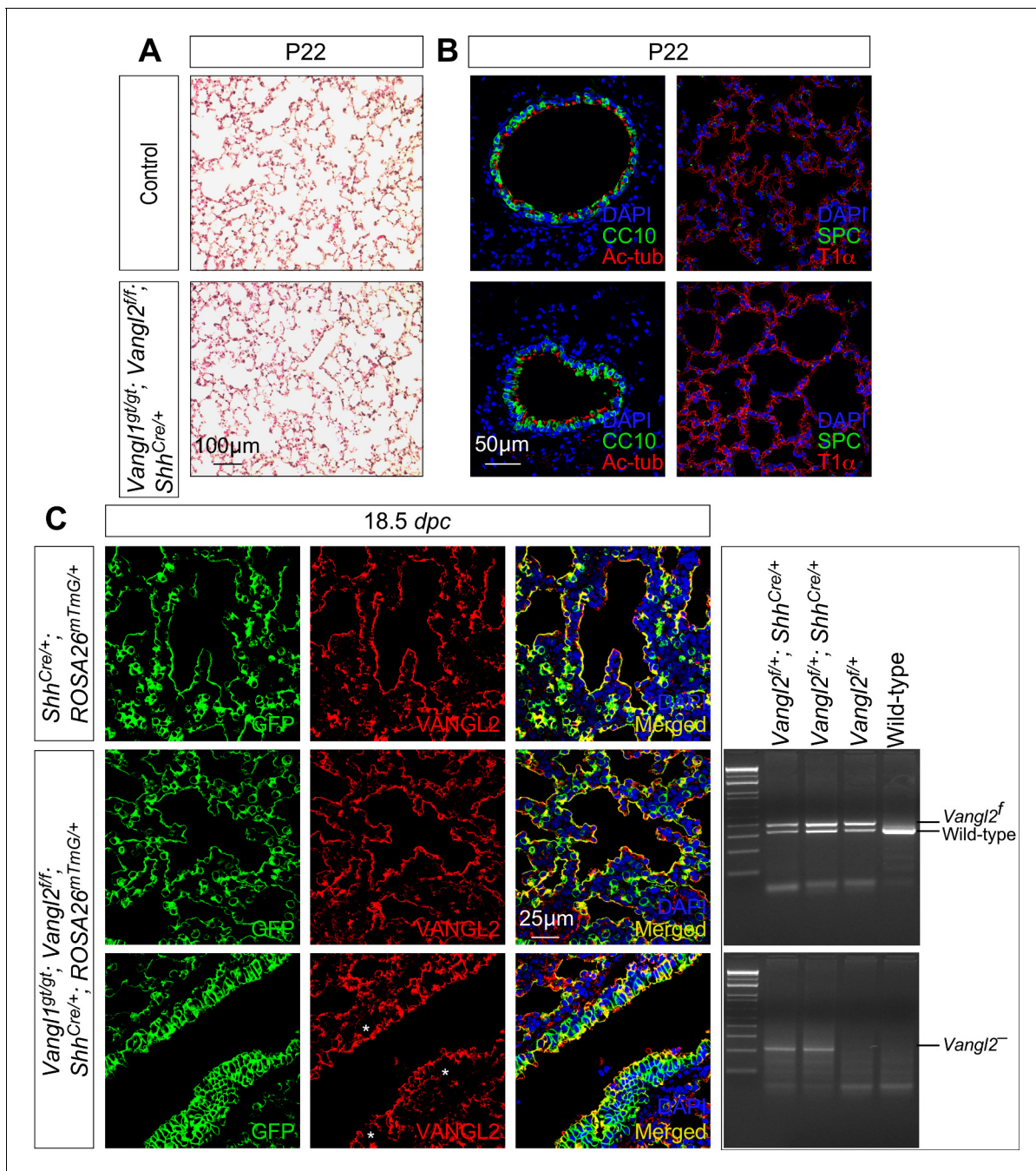


Figure 1—figure supplement 4. *Shh*-Cre fails to efficiently remove *Vangl2* in the lung epithelium. (A) Hematoxylin and eosin-stained lung sections of control and *Vangl1^{gt/gt}; Vangl2^{f/f}; Shh^{Cre/+}* mice at postnatal (P) day 22. Alveoli formed properly in *Vangl1^{gt/gt}; Vangl2^{f/f}; Shh^{Cre/+}* lungs, which were indistinguishable from control lungs. (B) Immunostaining of lung sections collected from control and *Vangl1^{gt/gt}; Vangl2^{f/f}; Shh^{Cre/+}* mice at P22. There was no discernable difference in cell type specification and distribution between control and *Vangl1^{gt/gt}; Vangl2^{f/f}; Shh^{Cre/+}* lungs. CC10 marked club (Clara) cells and Ac-tub marked ciliated cells in the airways. SPC labeled alveolar type II cells and T1α labeled alveolar type I cells in alveoli. (C) Immunostaining of lung sections collected from *Shh^{Cre/+}; ROSA26^{mTmG/+}* (control) and *Vangl1^{gt/gt}; Vangl2^{f/f}; Shh^{Cre/+}; ROSA26^{mTmG/+}* mice at 18.5 days post coitus (dpc). *Shh*-Cre induced epithelial GFP expression from the *ROSA26^{mTmG}* locus. Only small pockets (*) of the proximal lung epithelium in *Vangl1^{gt/gt}; Vangl2^{f/f}; Shh^{Cre/+}; ROSA26^{mTmG/+}* mice displayed VANGL2 loss in comparison with controls. This is consistent with the presence of *Vangl2⁻* (null) by PCR.

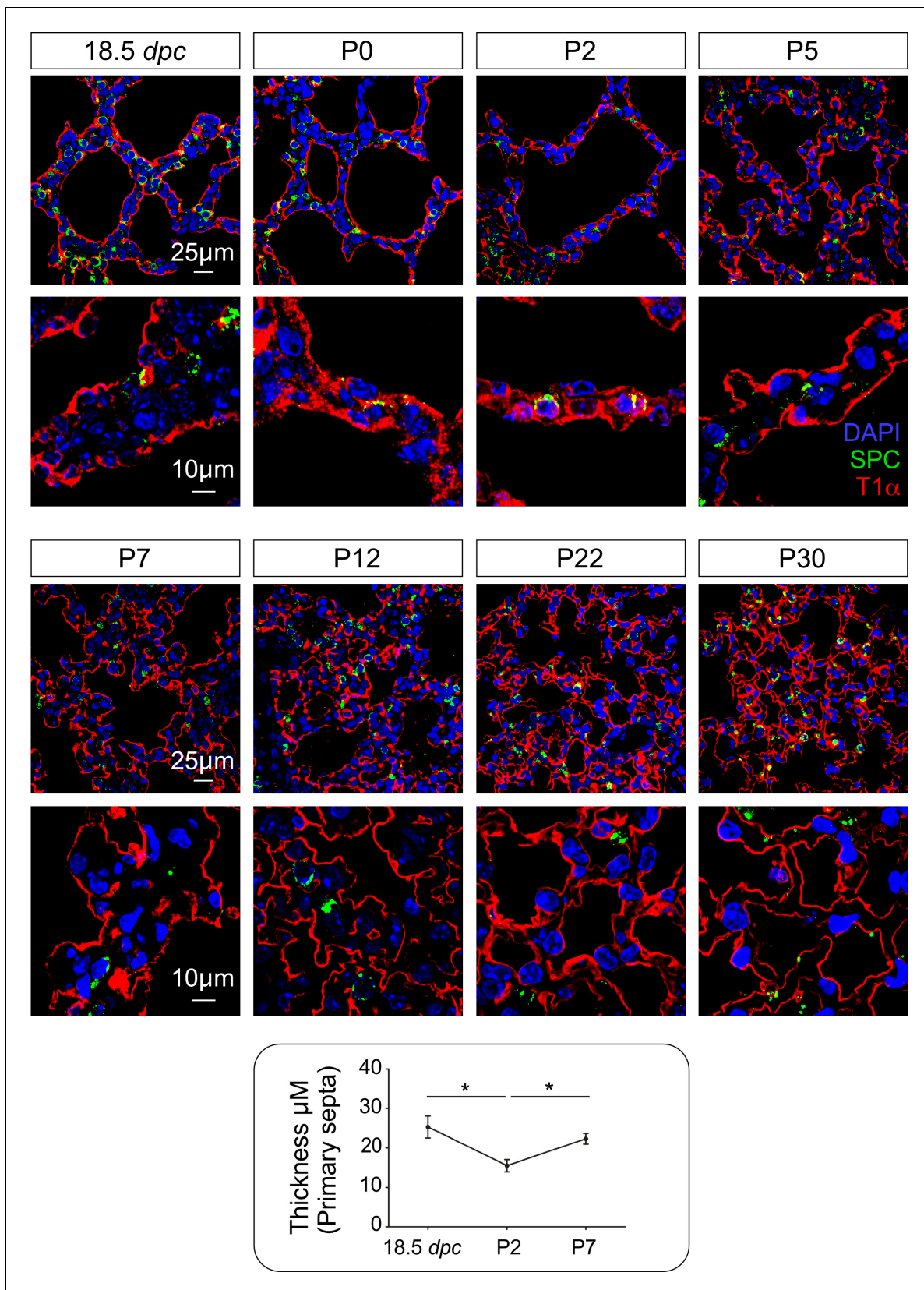


Figure 1—figure supplement 5. A time course of the development of the alveolar septa. Immunostaining of lung sections collected from wild-type mice at 18.5 days post coitus (dpc) and various postnatal (P) days as indicated. The primary septa appeared to be visibly thinner during the first three Figure 1—figure supplement 5 continued on next page

Figure 1—figure supplement 5 continued

days of postnatal life but its thickness increased subsequently. T1 α labeled alveolar type I cells while SPC marked alveolar type II cells. All values are mean SEM. (*) $p < 0.05$ (unpaired Student's t-test).

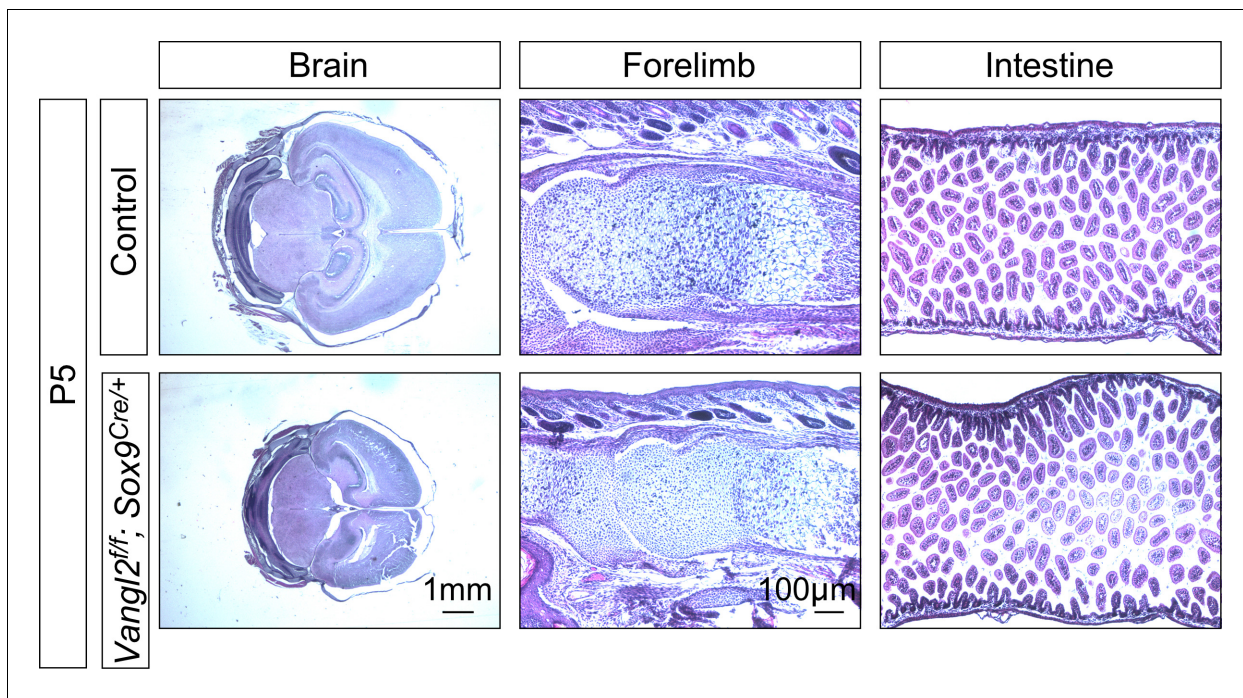


Figure 1—figure supplement 6. Histological analysis of tissues and organs in *Vangl2^{fl/fl}; Sox9^{Cre/+}* mice. Hematoxylin and eosin-stained tissue sections of control and *Vangl2^{fl/fl}; Sox9^{Cre/+}* mice at postnatal (P) day 5. Histological analysis revealed no apparent defects in the brain, bone and small intestine where *Sox9-Cre* is expressed.

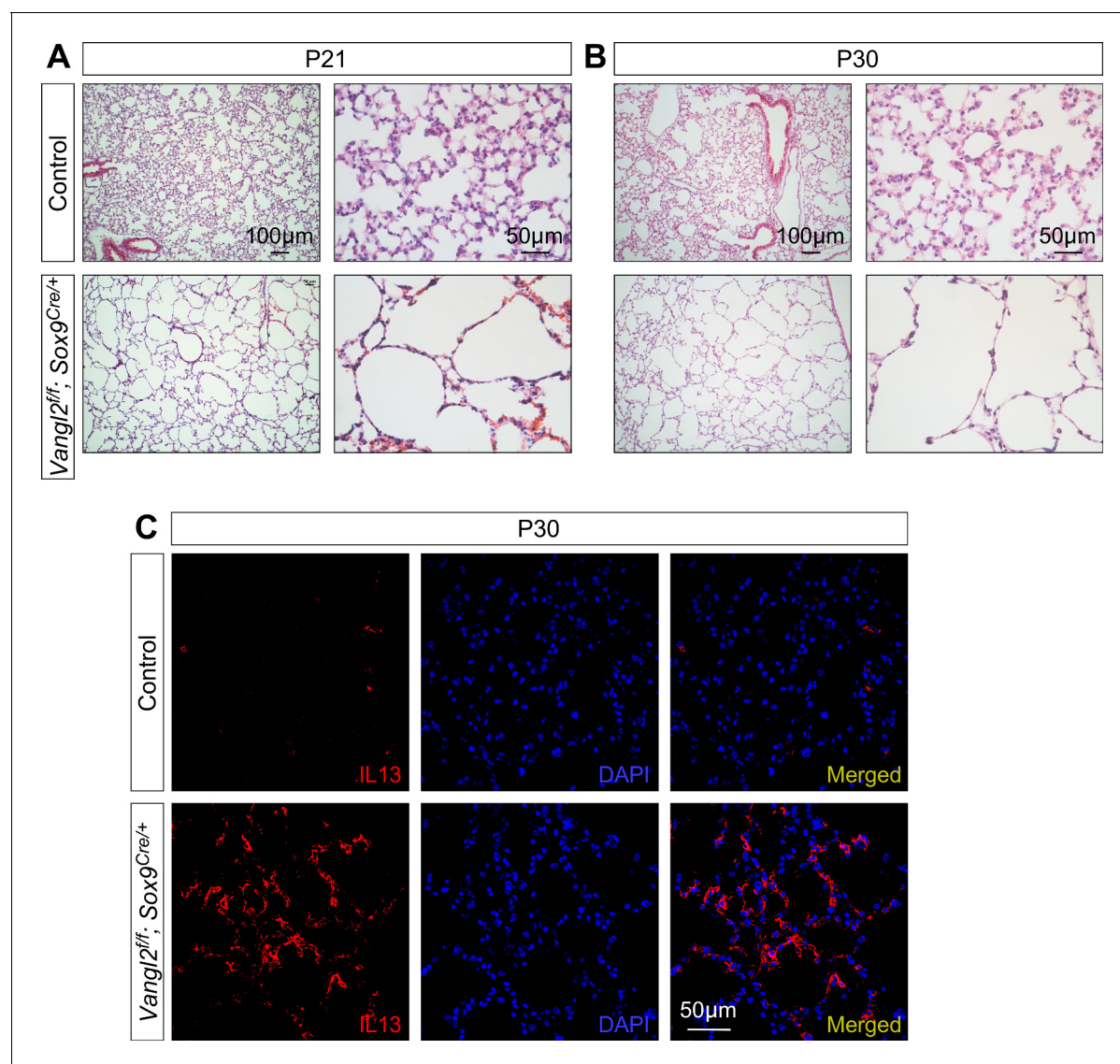


Figure 1—figure supplement 7. Loss of epithelial *Vangl2* disrupts secondary septa and alveolar formation. (A, B) Hematoxylin and eosin-stained lung sections of control and *Vangl2^{fl/fl}; Sox9^{Cre/+}* mice at postnatal (P) day 21 and 30. Secondary septa and alveoli failed to form and only thin primary septa persisted in *Vangl2^{fl/fl}; Sox9^{Cre/+}* lungs. (C) Immunostaining of lung sections collected from control and *Vangl2^{fl/fl}; Sox9^{Cre/+}* mice at P30. IL13 expression levels were elevated in the mutant lungs. Note that these *Vangl2^{fl/fl}; Sox9^{Cre/+}* animals were survivors since many of them succumbed to death prior to P10. No survivors beyond four weeks carry the genotype of *Vangl1^{gt/+}; Vangl2^{fl/fl}; Sox9^{Cre/+}*, consistent with a minor role of *Vangl1* in alveologenesis.

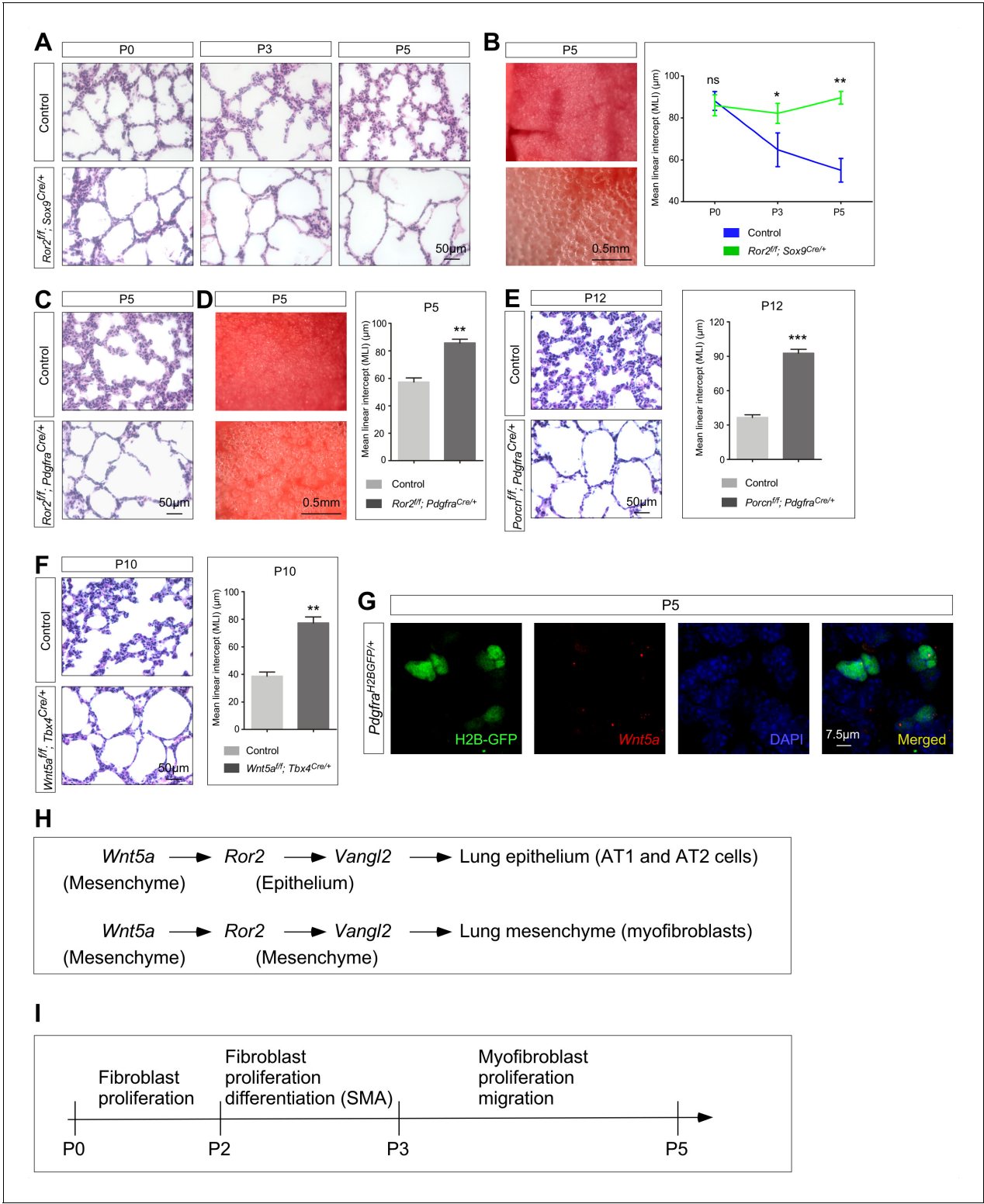


Figure 2. *Ror2* is required in both the lung epithelium and mesenchyme while *Wnt5a* is required in the lung mesenchyme for alveolar formation. (A) Hematoxylin and eosin-stained lung sections of wild-type and *Ror2^{fl/f}; Sox9^{Cre/+}* mice at different postnatal (P) stages. Histological analysis revealed the presence of enlarged saccules starting at P3 in *Ror2*-deficient lungs. (B) Surface view of dissected lungs from wild-type and *Ror2^{fl/f}; Sox9^{Cre/+}* mice at P5. Larger saccules were found in *Ror2* mutant lungs induced by *Sox9^{Cre}* and the MLI was correspondingly increased in *Ror2*-deficient lungs. (C) Hematoxylin and eosin-stained lung sections of wild-type and *Ror2^{fl/f}; Pdgfra^{Cre/+}* mice at P5. Histological analysis confirmed the presence of enlarged saccules starting at P3 in *Ror2*-deficient lungs. (D) Surface view of dissected lungs from wild-type and *Ror2^{fl/f}; Pdgfra^{Cre/+}* mice at P5. Larger saccules

Figure 2 continued on next page

Figure 2 continued

were found in *Ror2* mutant lungs induced by *Pdgfra*^{Cre} with an increased MLI. (E) Hematoxylin and eosin-stained lung sections of wild-type and *Porcn*^{f/f}; *Pdgfra*^{Cre/+} mice at P12. Larger saccules were found in *Porcn* mutant lungs induced by *Pdgfra*-Cre with an increased MLI. (F) Hematoxylin and eosin-stained lung sections of wild-type and *Wnt5a*^{f/f}; *Tbx4*^{Cre/+} mice at P10. Larger saccules were found in *Wnt5a* mutant lungs induced by *Tbx4*-Cre with an increased MLI. (G) Combined in situ hybridization (PLISH)/immunohistochemistry on lung sections of *Pdgfra*^{H2BGFP/+} mice to examine *Wnt5a* expression. *Wnt5a* mRNA was mainly detected in myofibroblasts (H2BGFP⁺) and not in the lung epithelium. (H) Schematic diagram of a *Wnt5a*–*Ror2*–*Vangl2* axis that functions in both the lung epithelium and mesenchyme to regulate alveologenesis. (I) Schematic diagram of the temporal sequence of fibroblast/myofibroblast proliferation, differentiation and migration.

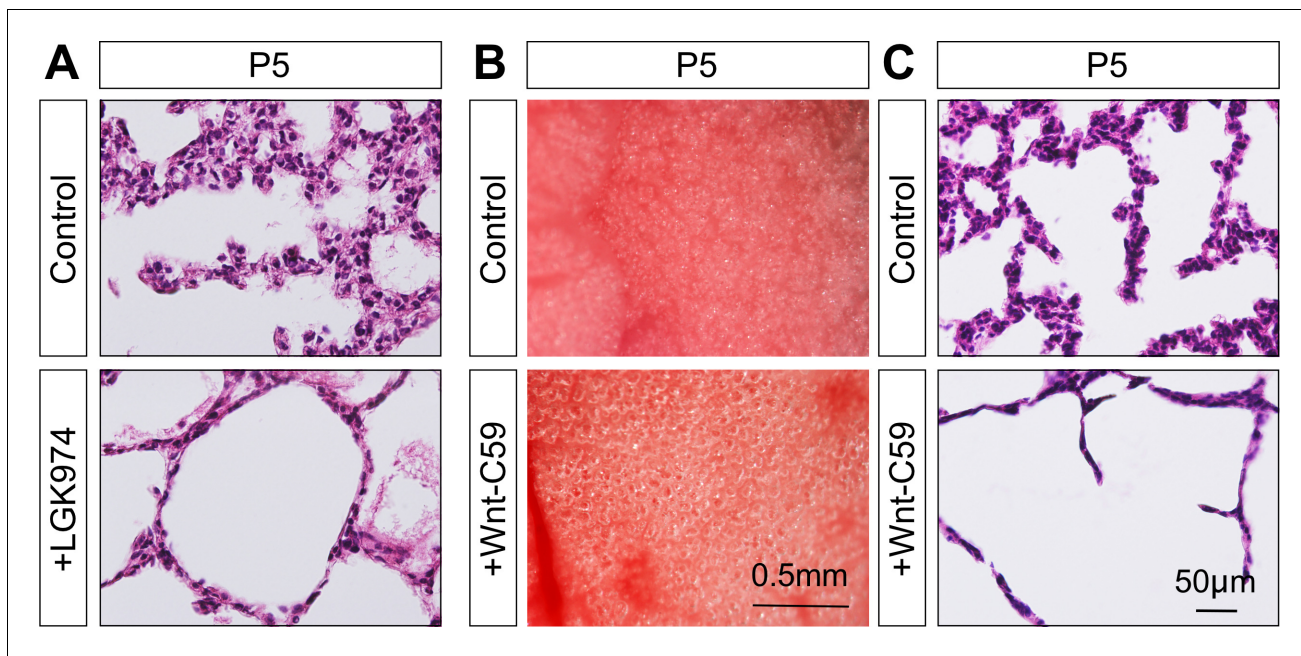


Figure 2—figure supplement 1. Inhibition of PORCUPINE activity leads to alveolar defects. (A) Hematoxylin and eosin-stained lung sections of mice at postnatal (P) day 5, which were treated with vehicles (control) or LGK974 (PORCUPINE inhibitor) at birth. (B) Surface view of dissected lungs from mice at P5, which were treated with vehicles or Wnt-C59 (PORCUPINE inhibitor) at birth. Larger saccules were found in lungs treated with Wnt-C59 compared to controls. (C) Histological analysis confirmed the presence of enlarged saccules in Wnt-C59-treated lungs.

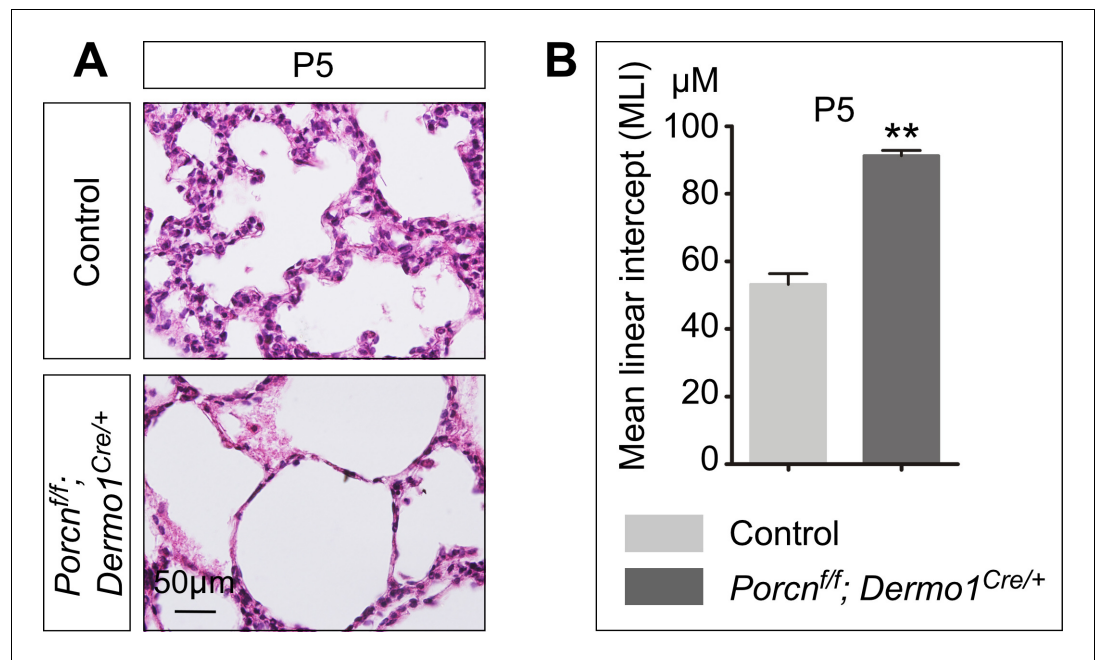


Figure 2—figure supplement 2. Elimination of mesenchymal *Porcupine* affects alveolar formation. (A) Hematoxylin and eosin-stained lung sections of control and *Porcn^{f/f}; Dermo1^{Cre/+}* mice at postnatal (P) day 5. Histological analysis revealed the presence of enlarged saccules in the absence of mesenchymal *Porcn* induced by *Dermo1*-Cre. (B) Measurement of the mean linear intercept (MLI) in control and *Porcn^{f/f}; Dermo1^{Cre/+}* lungs at P5. The MLI was increased in the mutant lungs. All values are mean SEM. (**) $p < 0.01$ (unpaired Student's *t*-test).

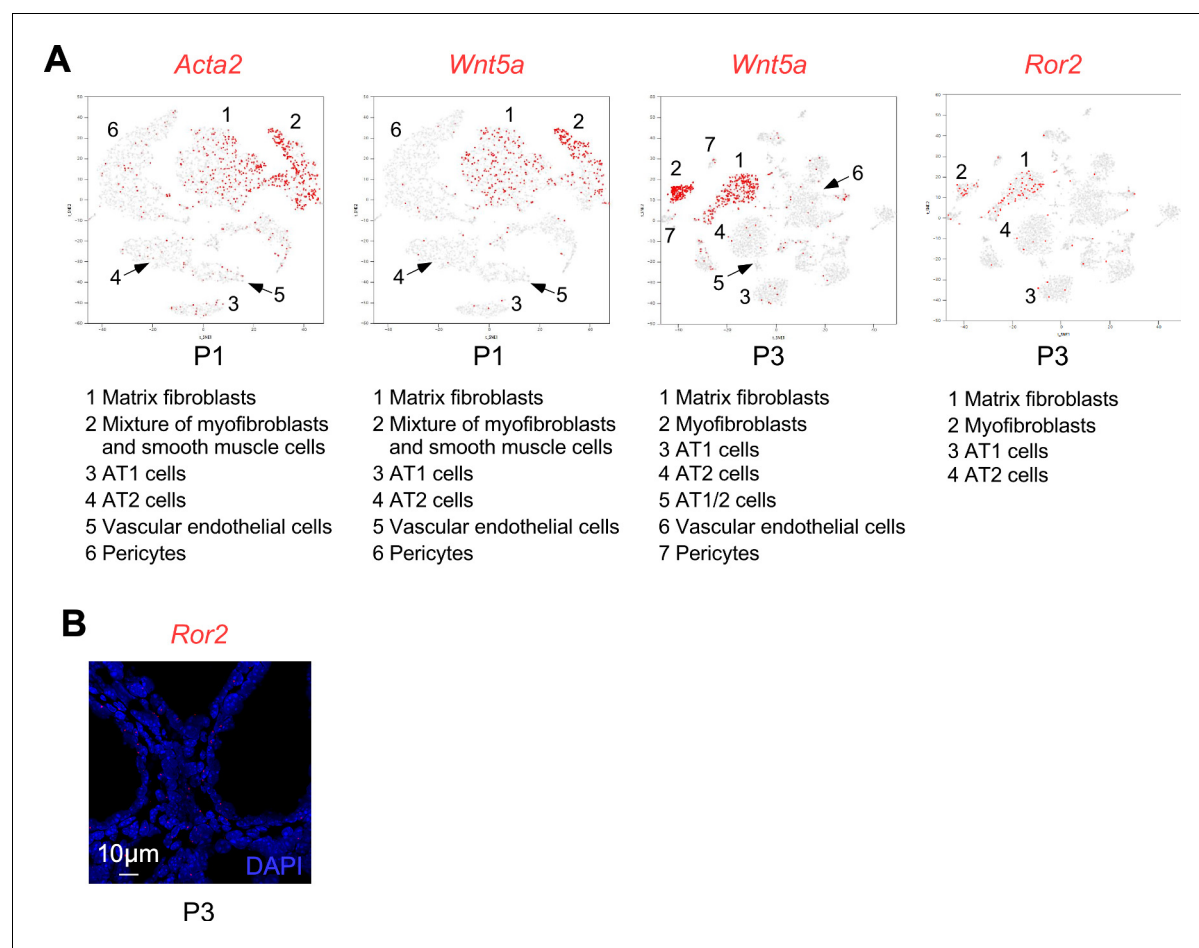


Figure 2—figure supplement 3. Single-cell RNA-Seq reveals expression of *Wnt5a* in myofibroblasts. (A) Single-cell RNA-Seq data of mouse lung cells at postnatal (P) 1 and 3 were downloaded from LungMAP, which is an NIH-funded consortium to generate publicly available data. Expression of *Acta2* (*SMA*), *Wnt5a* and *Ror2* (red color) was superimposed with predicted mouse lung cell populations on a t-SNE plot. At P1, *Wnt5a* is expressed in airway/vascular smooth muscle cells (*ACTA2*⁺) in addition to alveolar fibroblasts (*ACTA2*⁺). At P3, *Wnt5a* is highly expressed in fibroblasts and myofibroblasts but not in alveolar epithelial cells, endothelial cells or pericytes. At P3, *Ror2* is also highly expressed in fibroblasts and myofibroblasts with lower levels of expression in alveolar epithelial cells. (B) In situ hybridization (PLISH) on lung sections of wild-type mice to examine *Ror2* expression. *Ror2* was broadly expressed in both the lung epithelium and mesenchyme.

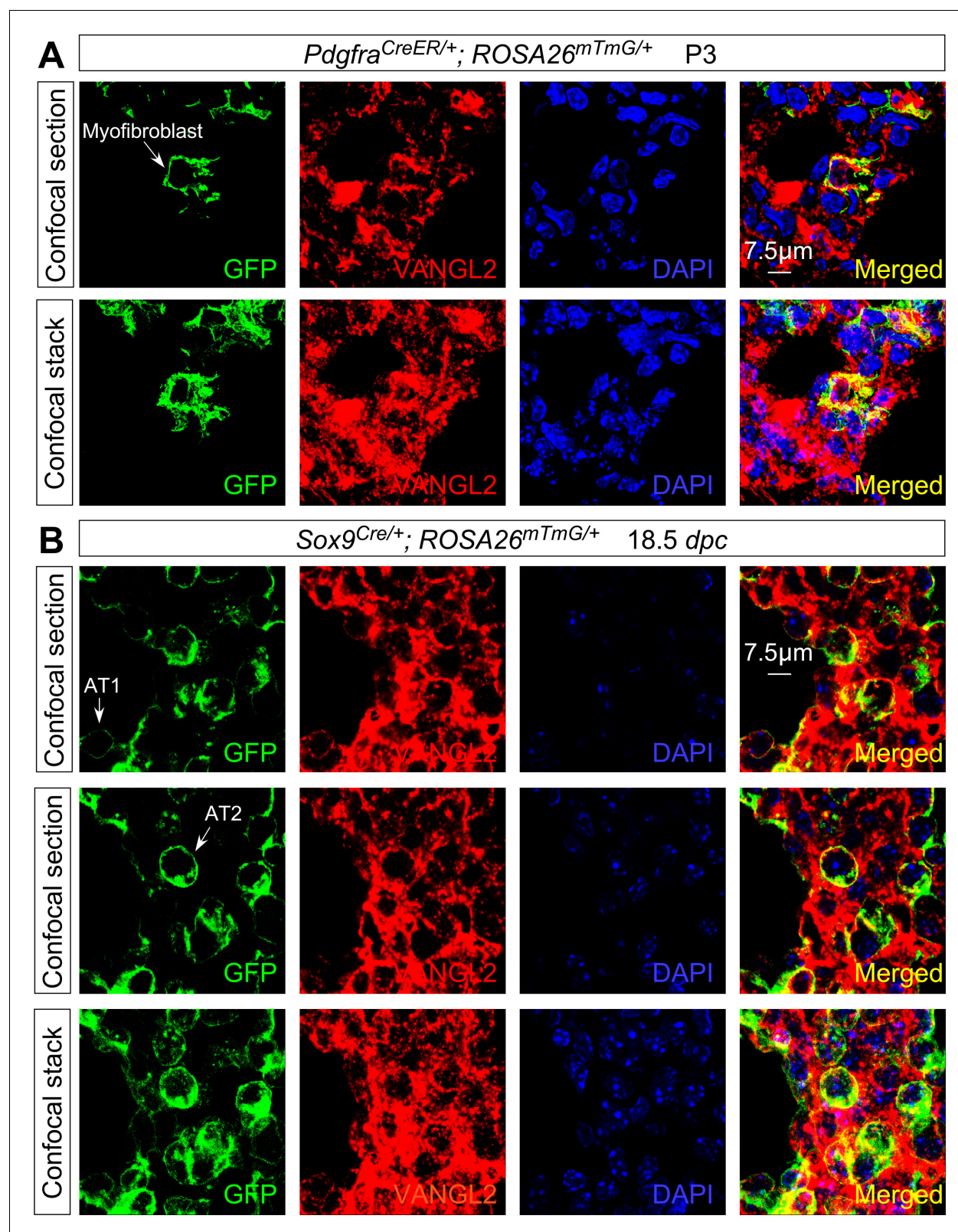


Figure 2—figure supplement 4. VANGL2 is not asymmetrically localized in lung epithelial and mesenchymal cells. (A) Immunostaining of lung sections collected from *Pdgfra*^{CreER/+}; *ROSA26*^{mTmG/+} mice at postnatal (P) day 3. Leaky expression of CreER led to GFP-labeling (from the *ROSA26*^{mTmG/+} locus) of individual myofibroblasts. No apparent asymmetric distribution of VANGL2 was detected in myofibroblasts. This was revealed by examining each confocal section. The confocal stack represents the compilation of all confocal sections for a given myofibroblast examined. (B) Immunostaining of

Figure 2—figure supplement 4 continued on next page

Figure 2—figure supplement 4 continued

lung sections collected from *Sox9^{Cre/+}; ROSA26^{mTmG/+}* mice at 18.5 days post coitus (*dpc*). Activation of GFP by *Sox9-Cre* resulted in labeling of alveolar type I (AT1) and type II (AT2) cells, which could be distinguished by morphology. No apparent asymmetric distribution of VANGL2 was detected in AT1 or AT2 cells. This was revealed by examining each confocal section. The confocal stack represents the compilation of all confocal sections for a given AT1 or AT2 cell examined. The extended morphology of AT1 cells placed an inherent limitation on the proportion of cell membrane that could be visualized in a given AT1 cell. Nevertheless, in regions that could be discerned, especially cell membranes surrounding the nucleus, no asymmetric distribution of VANGL2 was revealed.

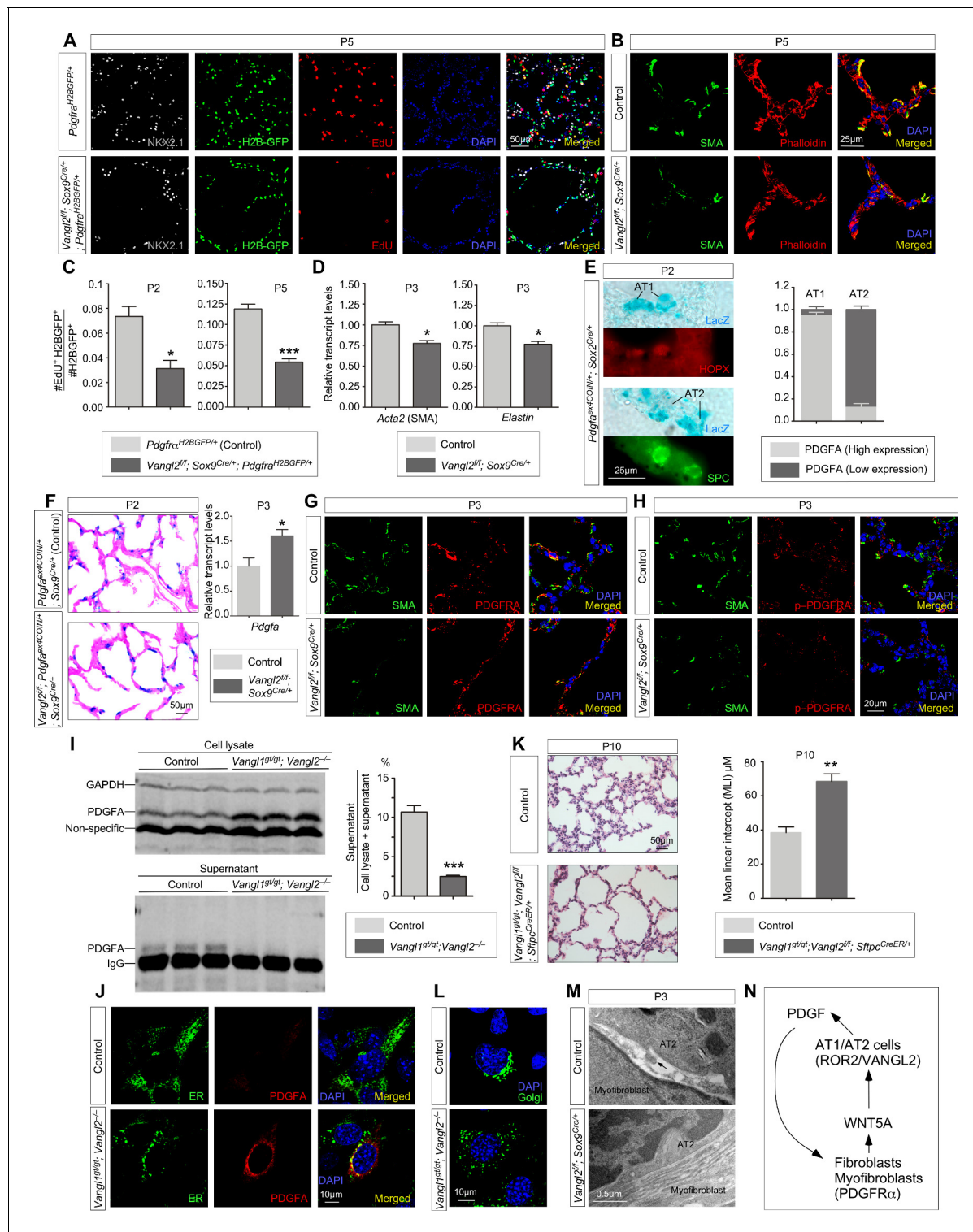


Figure 3. *Vangl2* is required for PDGF ligand trafficking/release from PDGF-producing cells and subsequently PDGF signal reception. (A) Immunostaining of lung sections collected from *Pdgfra*^{H2BGFP/+} (control) and *Vangl2*^{fl/fl}; *Sox9*^{Cre/+}; *Pdgfra*^{H2BGFP/+} mice injected with EdU at postnatal (P) day 5. Lung epithelial cells were distinguished by NKX2.1 staining while myofibroblasts were marked by H2B-GFP from the *Pdgfra* locus (*Pdgfra*^{H2BGFP}). The number of EdU⁺ cells was reduced in *Vangl2*^{fl/fl}; *Sox9*^{Cre/+}; *Pdgfra*^{H2BGFP/+} lungs compared to controls. (B) Immunostaining of lung sections collected from control and *Vangl2*^{fl/fl}; *Sox9*^{Cre/+} mice at P5. Organization of the cytoskeleton and stress fibers was disrupted and SMA at the prospective sites of secondary septation was sparse in *Vangl2*-deficient lungs. (C) Quantification of myofibroblast proliferation in *Pdgfra*^{H2BGFP/+} (control) and *Vangl2*^{fl/fl}; *Sox9*^{Cre/+}; *Pdgfra*^{H2BGFP/+} lungs at P2 and P5. The rate of myofibroblast proliferation was calculated as the ratio of the number of EdU⁺ cells. Figure 3 continued on next page

Figure 3 continued

myofibroblasts (EdU⁺H2BGFP⁺) to the number of myofibroblasts (H2BGFP⁺). An apparent reduction in the percentage of proliferating myofibroblasts was detected in *Vangl2^{fl/fl}; Sox9^{Cre/+}; Pdgfra^{H2BGFP/+}* lungs compared to controls (n = 3 for each group) at P2 and P5. (D) qPCR analysis of *Acta2* (SMA) and *Elastin* in control and *Vangl2^{fl/fl}; Sox9^{Cre/+}* lungs at P3. The mRNA levels of *Acta2* and *Elastin* were significantly reduced in the absence of epithelial *Vangl2* induced by *Sox9*-Cre (n = 3 for each group). (E) Immunostaining of lung sections collected from *Pdgfa^{ex4COIN/+}; Sox2^{Cre/+}* mice at P2. β -galactosidase (LacZ) was induced in PDGFA-producing cells by *Sox2*-Cre. LacZ-staining (blue) was followed by immunostaining against HOPX (marker for AT1 cells) and SPC (marker for AT2 cells). LacZ-positive cells also expressed either HOPX or SPC. The number of AT1 or AT2 cells that harbored either high or low PDGFA (LacZ) was counted. (F) LacZ-staining (blue) of lung sections collected from *Pdgfa^{ex4COIN/+}; Sox9^{Cre/+}* (control) and *Vangl2^{fl/fl}; Pdgfa^{ex4COIN/+}; Sox9^{Cre/+}* mice at P2. The slides were counterstained with eosin (red). No difference in the intensity of LacZ (+) cells in the lung was found in these two mouse lines. The mRNA levels of *Pdgfa* in control and mutant lungs were determined by qPCR. (G) Immunostaining of lung sections collected from control and *Vangl2^{fl/fl}; Sox9^{Cre/+}* mice at P3. No difference in PDGFRA expression levels in individual myofibroblasts was noted between control and *Vangl2^{fl/fl}; Sox9^{Cre/+}* lungs. (H) Immunostaining of lung sections collected from control and *Vangl2^{fl/fl}; Sox9^{Cre/+}* mice at P3. A significant reduction in the levels of phosphorylated (p) PDGFRA in individual myofibroblasts was found in *Vangl2^{fl/fl}; Sox9^{Cre/+}* lungs compared to controls. (I) Western blot analysis of cell lysates and supernatants from control and *Vangl1^{gt/gt}; Vangl2^{-/-}* cells lentivirally transduced with PDGFA-expressing constructs. The amount of PDGFA released into the media was significantly reduced in *Vangl1^{gt/gt}; Vangl2^{-/-}* cells compared to controls (n = 3 for each group). GAPDH served as a loading control. We noticed that the amount of secreted proteins (normalized to the cell number) from *Vangl1/2* mutant cells was reduced compared to controls. This suggests a general defect in protein processing/secretion in the absence of *Vangl1/2*. In this case, it is possible that other secreted ligands could also impact alveolar development. (J) Immunostaining of controls and *Vangl1^{gt/gt}; Vangl2^{-/-}* cells lentivirally transduced with PDGFA-expressing constructs. Endoplasmic reticulum (ER) was marked by mEmerald-ER-5. (K) Hematoxylin and eosin-stained lung sections of wild-type and *Vangl1^{gt/gt}; Vangl2^{fl/fl}; Sftpc^{CreER/+}* mice injected with tamoxifen and collected at P10. Enlarged saccules were found in *Vangl1^{gt/gt}; Vangl2^{fl/fl}; Sftpc^{CreER/+}* lungs in comparison with controls. (L) Immunostaining of controls and *Vangl1^{gt/gt}; Vangl2^{-/-}* cells. The Golgi stacks were dispersed in *Vangl1^{gt/gt}; Vangl2^{-/-}* cells compared to controls. Golgi was marked by mEmerald-Golgi-7. (M) Transmission electron micrographs of lungs from wild-type and *Vangl2^{fl/fl}; Sox9^{Cre/+}* mice at P3. Cellular extension (arrow) from alveolar type II cells to myofibroblasts was observed in control lungs but were absent in *Vangl2^{fl/fl}; Sox9^{Cre/+}* lungs. (N) Schematic diagram of a positive feedback loop between WNT5A and PDGF to generate a pool of fibroblasts/myofibroblasts for alveologenesis. All values are mean \pm SEM. (*) p<0.05; (**) p<0.01; (***) p<0.001; ns, not significant (unpaired Student's t-test).

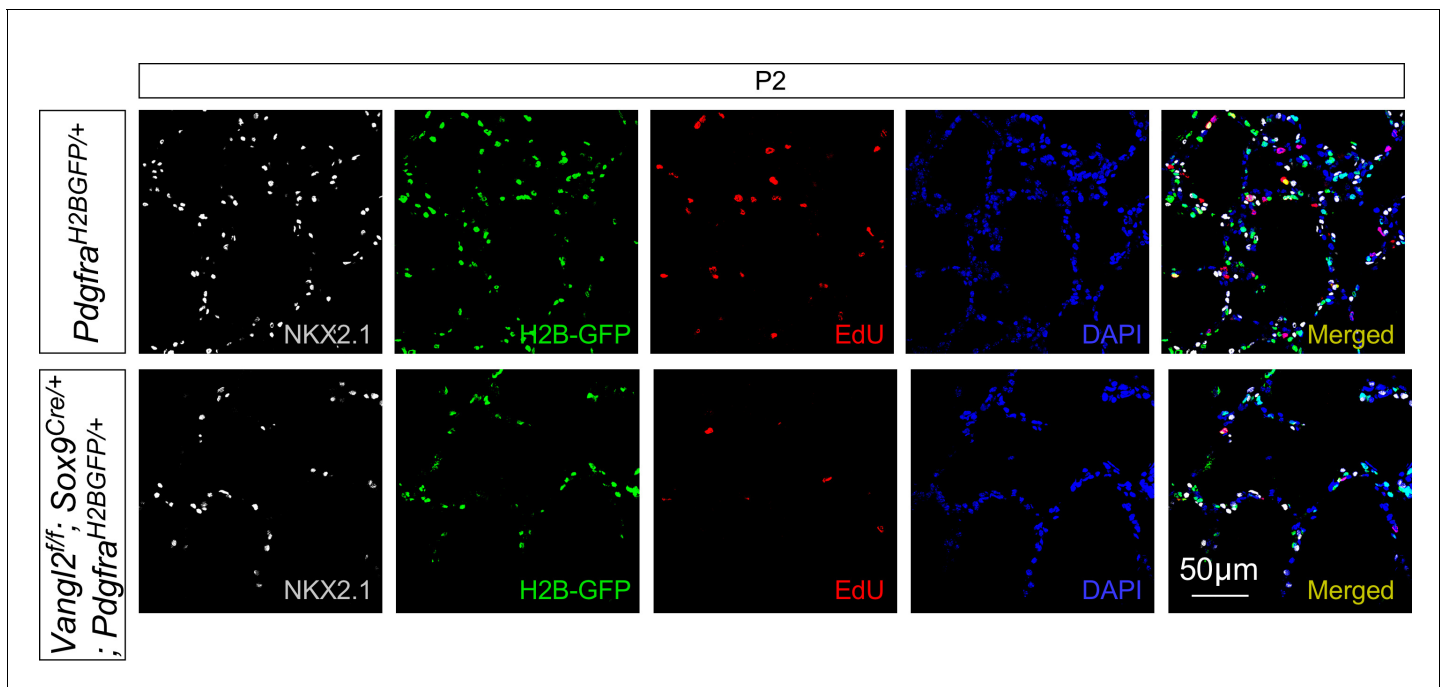


Figure 3—figure supplement 1. Loss of epithelial *Vangl2* leads to reduced myofibroblast proliferation. Immunostaining of lung sections collected from *Pdgfra*^{H2BGFP/+} (control) and *Vangl2^{fl/fl}; Sox9^{Cre/+}; Pdgfra^{H2BGFP/+}* mice injected with EdU at postnatal (P) day 2. Lung epithelial cells were distinguished by NKX2.1 staining while myofibroblasts were marked by H2B-GFP from the *Pdgfra* locus (*Pdgfra*^{H2BGFP}). The number of EdU⁺ cells was reduced in *Vangl2^{fl/fl}; Sox9^{Cre/+}; Pdgfra^{H2BGFP/+}* lungs compared to controls. Note that quantification of proliferating myofibroblasts (EdU⁺H2BGFP⁺) is shown in **Figure 3C**.

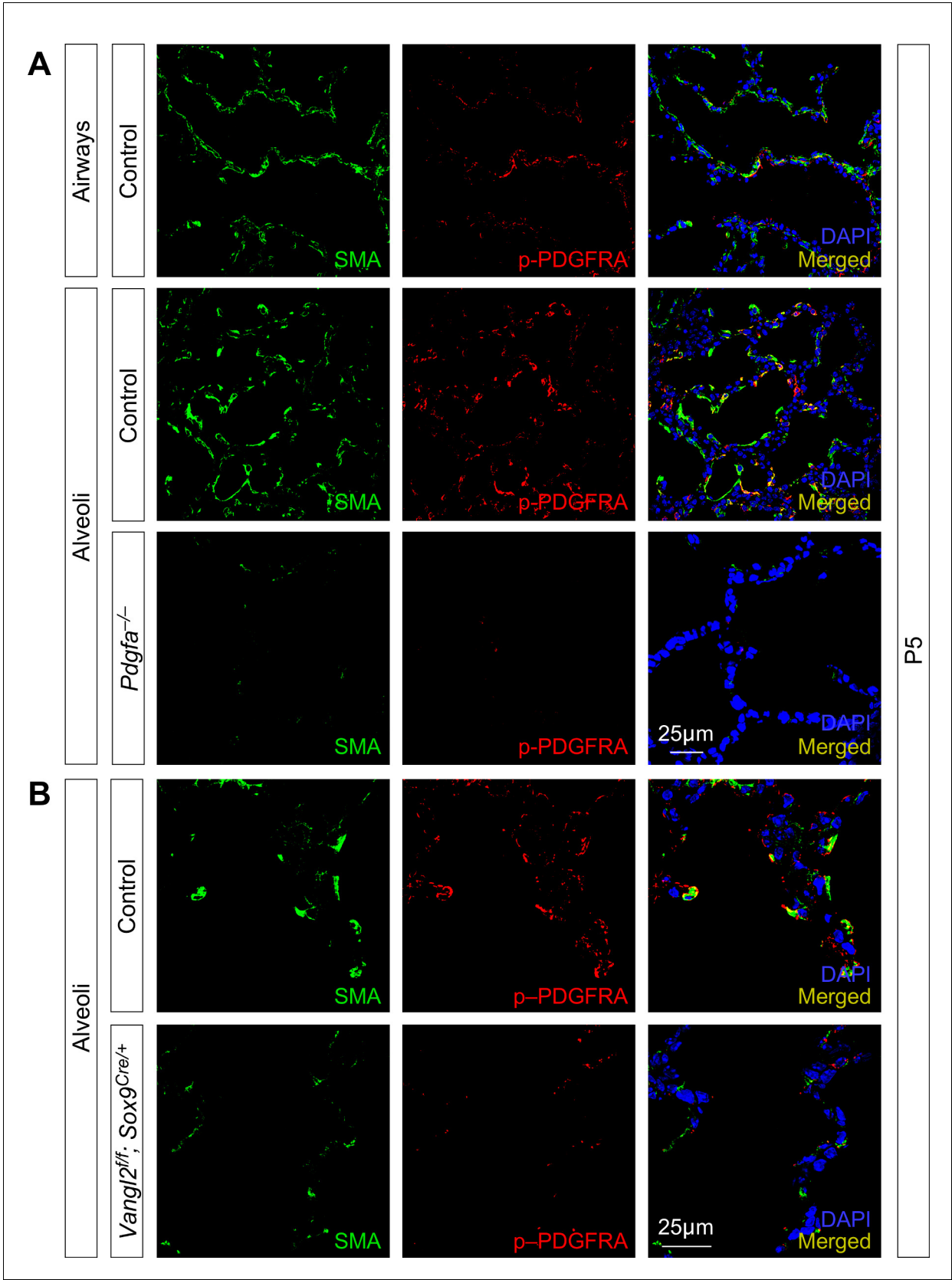


Figure 3—figure supplement 2. Removal of epithelial *Vangl2* results in reduced levels of phosphorylated PDGFRα. (A) Immunostaining of lung sections collected from control and *Pdgfa*^{ex4COIN/ex4COIN}; *Sox2*^{Cre/+} (abbreviated as *Pdgfa*^{-/-}) mice at postnatal (P) day 5. PDGFRα⁺ myofibroblasts were

Figure 3—figure supplement 2 continued on next page

Figure 3—figure supplement 2 continued

absent in *Pdgfra*^{-/-} lungs. Accordingly, phosphorylated (p) PDGFRA (p-PDGFRA) was barely detectable in *Pdgfra*^{-/-} lungs. **(B)** Immunostaining of lung sections collected from control and *Vangl2*^{fl/fl}; *Sox9*^{Cre/+} mice at P5. A significant reduction in the levels of p-PDGFRA in individual myofibroblasts was found in *Vangl2*^{fl/fl}; *Sox9*^{Cre/+} lungs compared to controls. Smooth muscle actin (SMA) was primarily detected in smooth muscles and myofibroblasts.

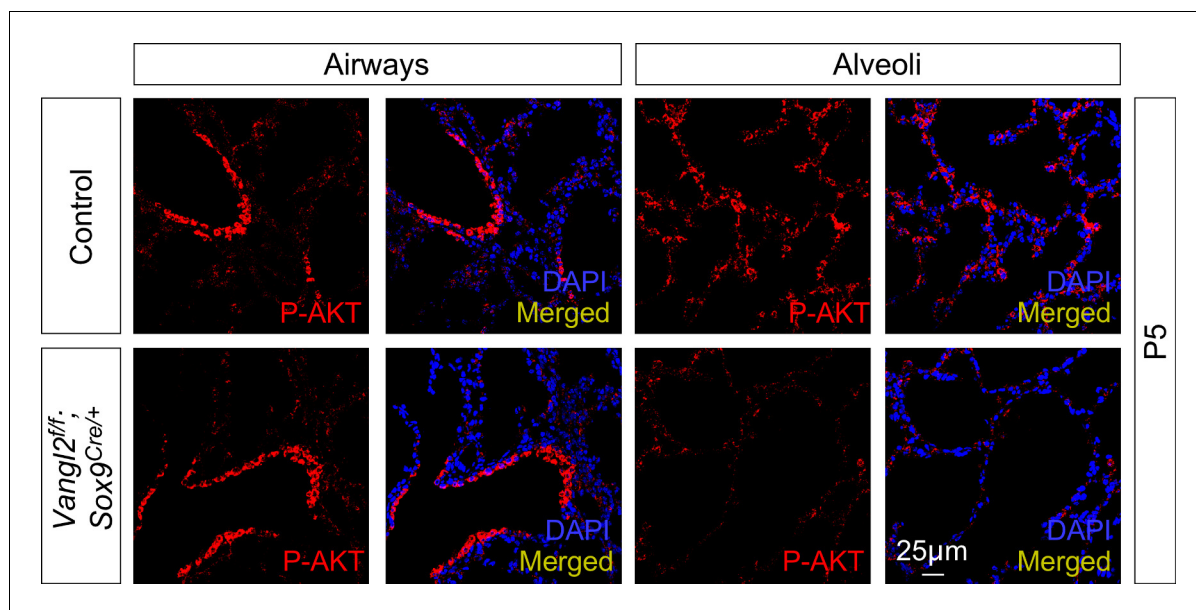


Figure 3—figure supplement 3. PDGF signal reception is reduced in lungs deficient in *Vangl1/2* signaling. Immunostaining of lung sections collected from control and *Vangl2^{fl/fl}; Sox9^{Cre/+}* mice at postnatal (P) day 5. While phosphorylated (p) AKT (p-AKT) showed no difference between control and *Vangl2^{fl/fl}; Sox9^{Cre/+}* lungs in the airways, p-AKT levels were significantly reduced in the alveoli of *Vangl2^{fl/fl}; Sox9^{Cre/+}* mice.

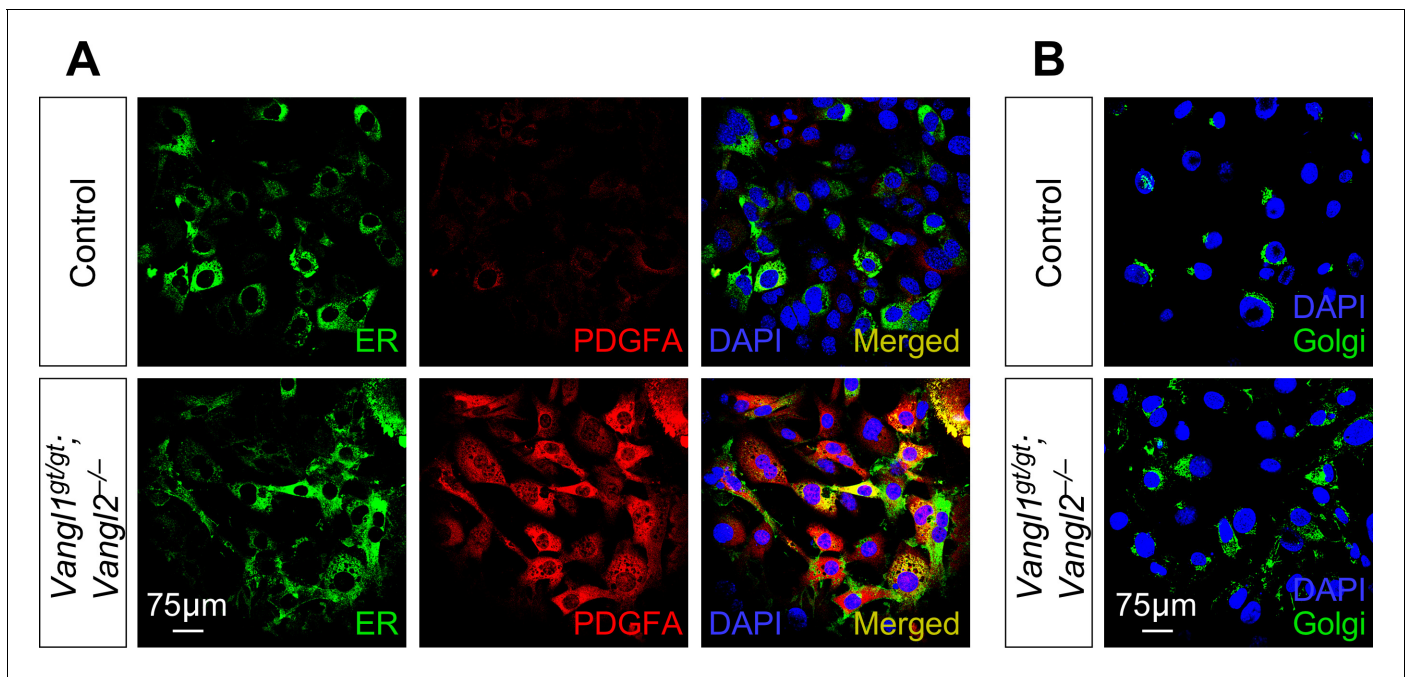


Figure 3—figure supplement 4. Accumulation of PDGF ligand in the secretory pathway in the absence of VANGL1/2. (A) Immunostaining of controls and *Vangl1^{gt/gt}; Vangl2^{-/-}* cells lentivirally transduced with PDGFA-expressing constructs. Endoplasmic reticulum (ER) was marked by mEmerald-ER-5. The levels of PDGFA were significantly increased in the secretory pathway of *Vangl1/2*-deficient cells. (B) Immunostaining of controls and *Vangl1^{gt/gt}; Vangl2^{-/-}* cells lentivirally transduced with PDGFA-expressing constructs. Golgi was marked by mEmerald-Golgi-7. The Golgi stacks were dispersed in *Vangl1/2*-deficient cells.

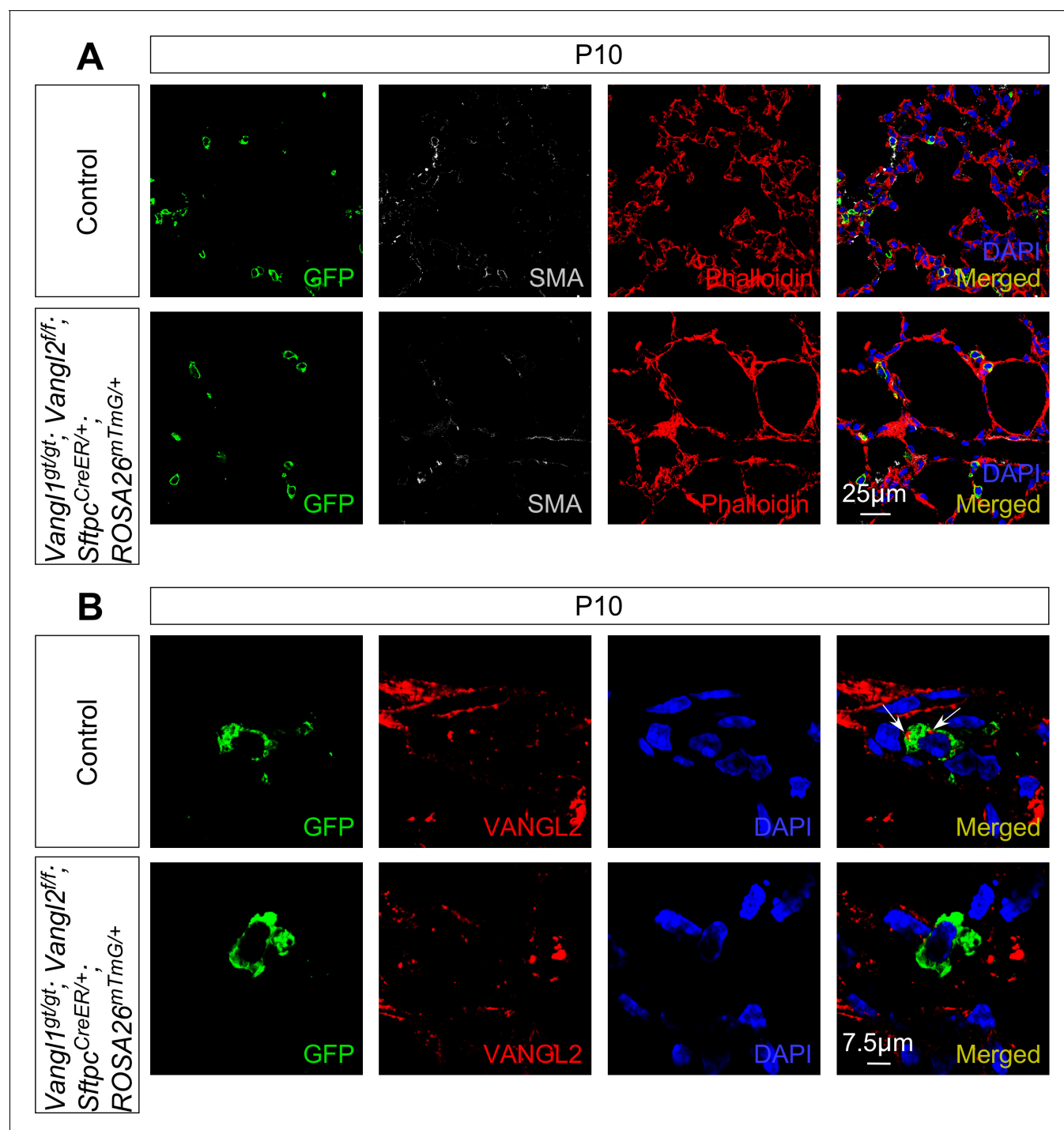


Figure 3—figure supplement 5. Loss of *Vangl1/2* in alveolar type II cells results in alveolar defects. (A) Immunostaining of lung sections collected from control and *Vangl1^{gt/gt}; Vangl2^{f/f}; Sftpc^{CreER/+}; ROSA26^{mTmG/+}* mice at postnatal (P) day 10. Tamoxifen was administered at P0. Inactivation of *Vangl1/2* in alveolar type II (AT2) cells led to alveolar defects. (B) Immunohistochemical analysis of lung sections collected from control and *Vangl1^{gt/gt}; Vangl2^{f/f}; Sftpc^{CreER/+}; ROSA26^{mTmG/+}* mice revealed loss of VANGL2 in AT2 cells (GFP⁺) in the mutant lungs.

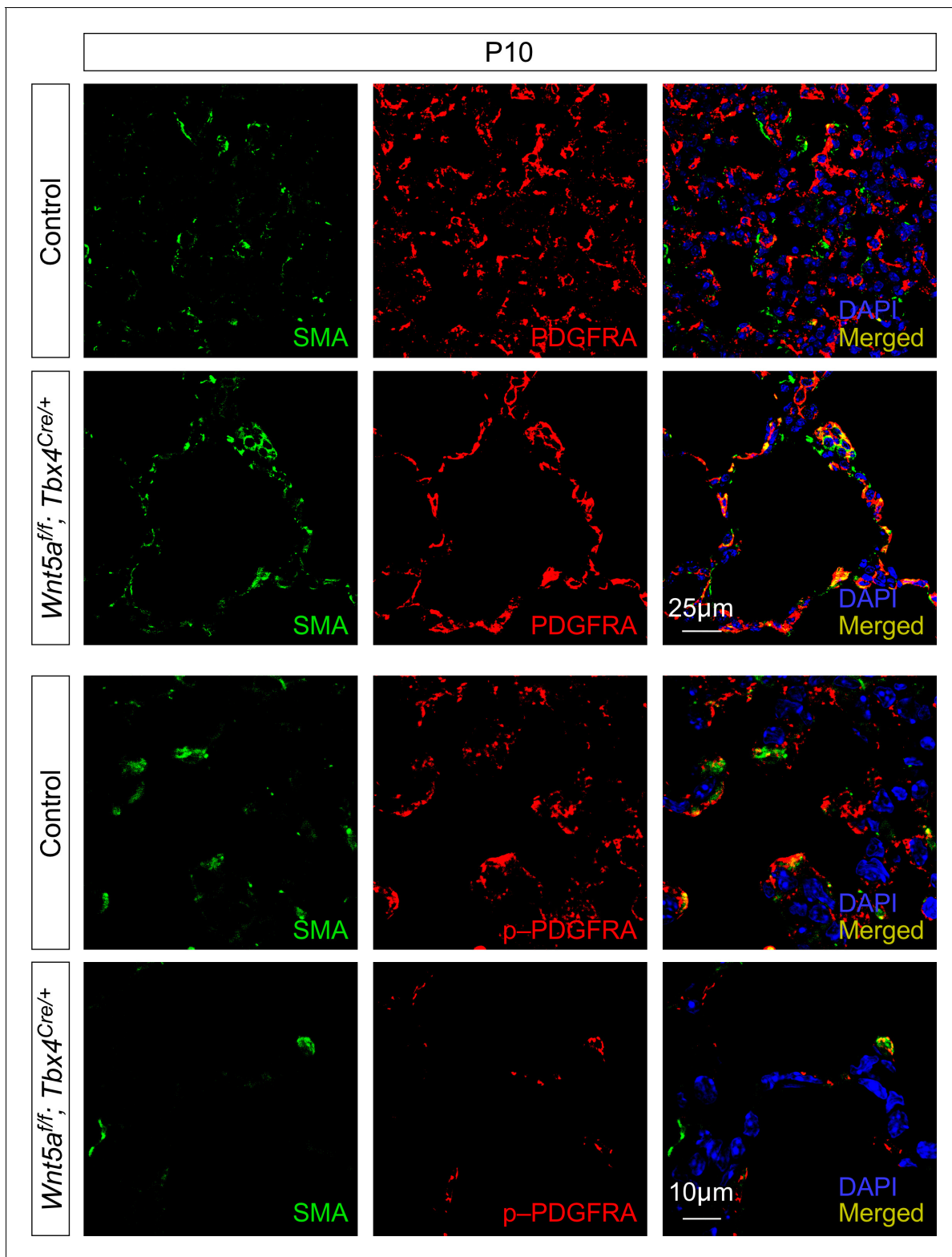


Figure 3—figure supplement 6. Removal of mesenchymal *Wnt5a* results in reduced levels of phosphorylated PDGFRA. Immunostaining of lung sections collected from control and *Wnt5a^{fl/fl}; Tbx4^{Cre/+}* mice at postnatal (P) day 10. A significant reduction in the levels of phosphorylated (p) PDGFRA in individual myofibroblasts was found in *Wnt5a^{fl/fl}; Tbx4^{Cre/+}* lungs compared to controls. By contrast, the levels of PDGFRA in individual myofibroblasts were unaffected.

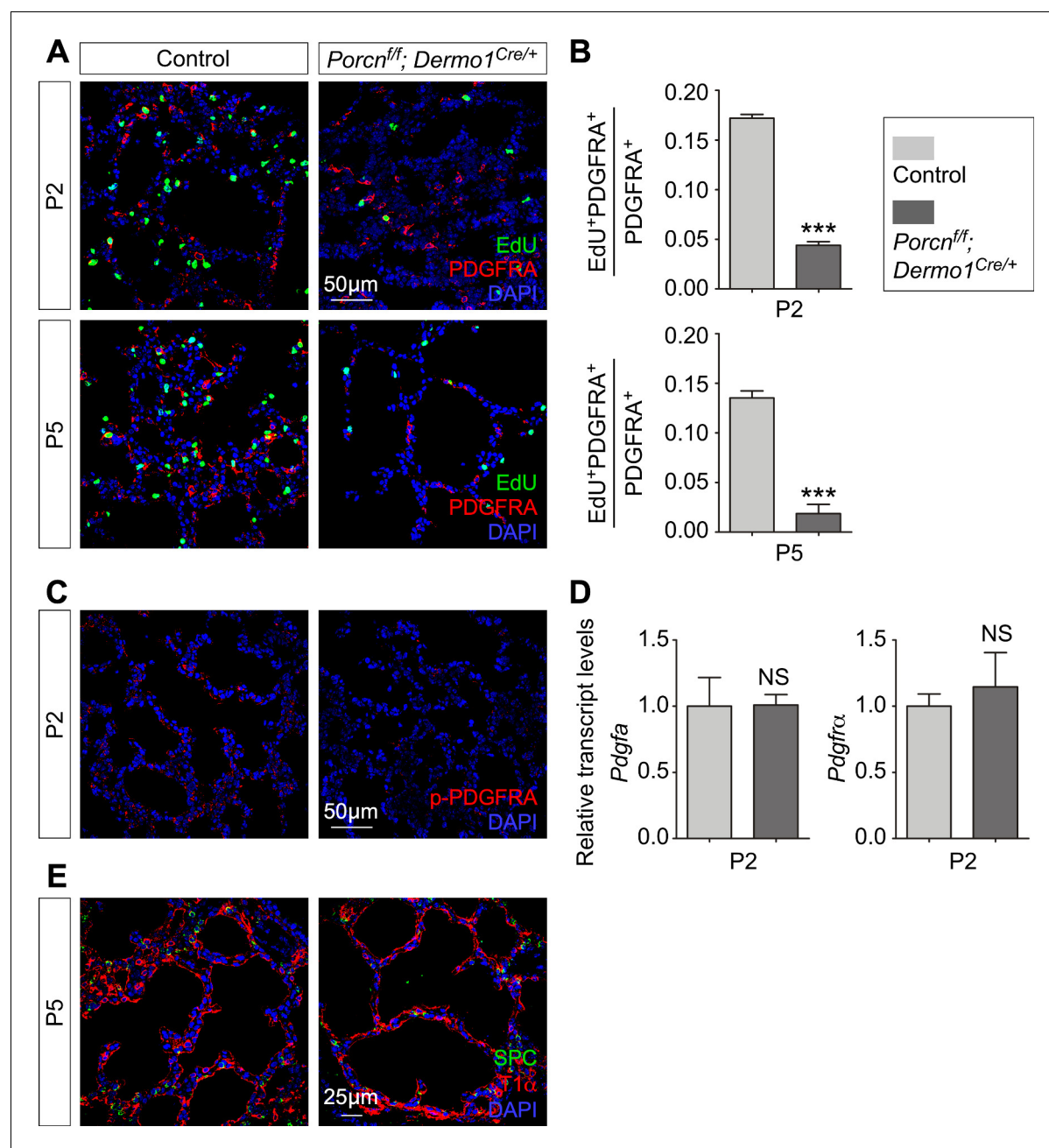


Figure 3—figure supplement 7. Mesenchymal Wnt signaling is required for fibroblast/myofibroblast proliferation but does not affect differentiation of alveolar epithelial cells. (A, C, E) Immunostaining of lung sections from control and *Porcn^{f/f}; Dermo1^{Cre/+}* mice at postnatal (P) day 2 and 5. The number of proliferating myofibroblasts (EdU⁺PDGFRA⁺) was reduced in the absence of mesenchymal Wnt signaling (shown in A). Quantification (n = 3 for each group) was shown in (B). Phosphorylated (p) PDGFRA was significantly reduced in the mutant lungs (shown in C) while the transcript levels of *Pdgfa* and *Pdgfra* were unaltered (n = 3 for each group) (shown in D). Loss of mesenchymal Wnt signaling had no effect on differentiation of alveolar epithelial cells (shown in E). All values are mean SEM. (***) p<0.001; ns, not significant (unpaired Student's t-test).

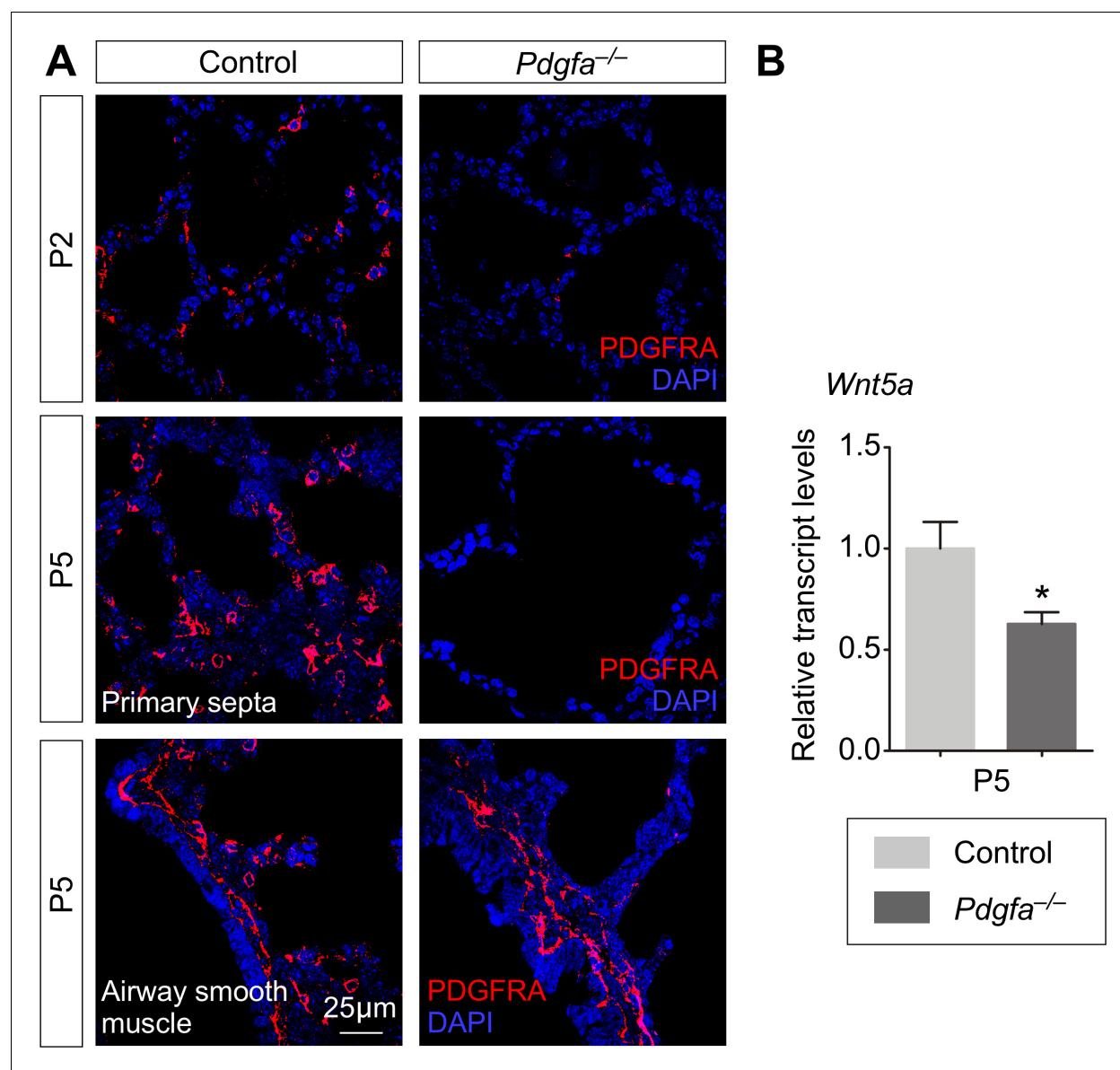


Figure 3—figure supplement 8. PDGF signaling is required for preserving a pool of WNT5A-secreting myofibroblasts. (A) Immunostaining of lung sections collected from control and *Pdgfa*^{ex4COIN/ex4COIN; Sox2^{Cre/+}} (abbreviated as *Pdgfa*^{-/-}) mice at postnatal (P) day 2 and 5. PDGFRA⁺ myofibroblasts were absent in *Pdgfa*^{-/-} lungs. This indicates that the source of WNT5A (produced from myofibroblasts) for alveolar development was depleted. By contrast, PDGFRA⁺ smooth muscle cells in the airway were unaffected in the absence of PDGF signaling. (B) qPCR analysis of *Wnt5a* transcript levels in control and *Pdgfa*^{-/-} lungs (n = 4) at P5. *Wnt5a* mRNA levels were reduced in the absence of PDGF signaling. All values are mean SEM. (*) p<0.05. (unpaired Student's *t*-test).

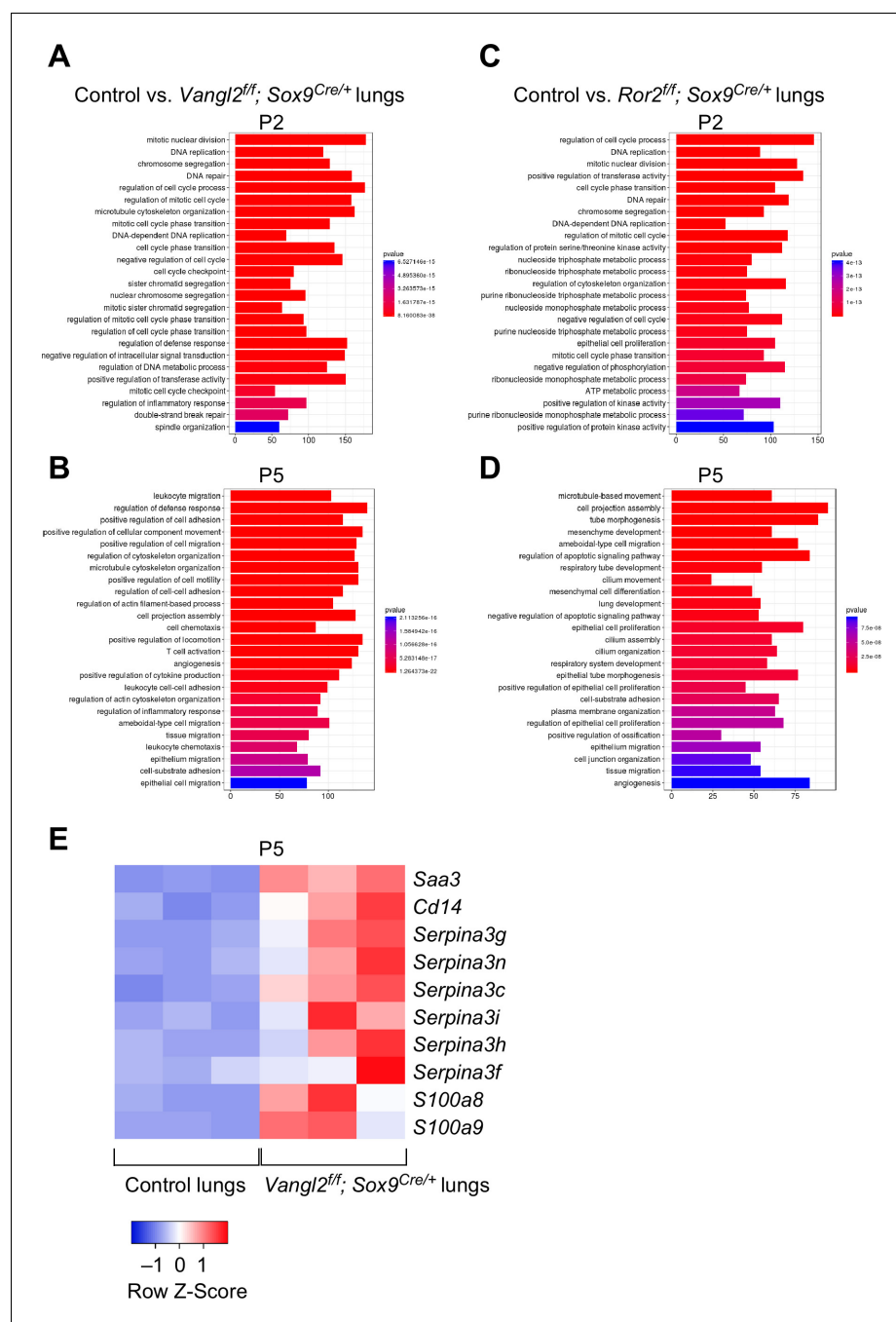


Figure 4. *Vangl2* and *Ror2* regulate similar pathways. (A–D) Pathway analysis of transcriptomes derived from RNA-Seq of control, *Vangl2^{fl/fl}; Sox9^{Cre/+}*, and *Ror2^{fl/fl}; Sox9^{Cre/+}* lungs at postnatal (P) day 2 and 5 (n = 3 for each group). The top 25 enriched terms in GO (gene ontology) biological processes were shown. Loss of *Vangl2* or *Ror2* revealed changes in similar pathways, suggesting that *Vangl2* and *Ror2* function in the same pathway. (E) Heatmap of selected mouse genes from control and *Vangl2^{fl/fl}; Sox9^{Cre/+}* lungs at P5. Loss of epithelial *Vangl2* in mouse lungs activated these genes. Interestingly, they are known to be elevated in lungs of human emphysema patients and are biomarkers for emphysema.

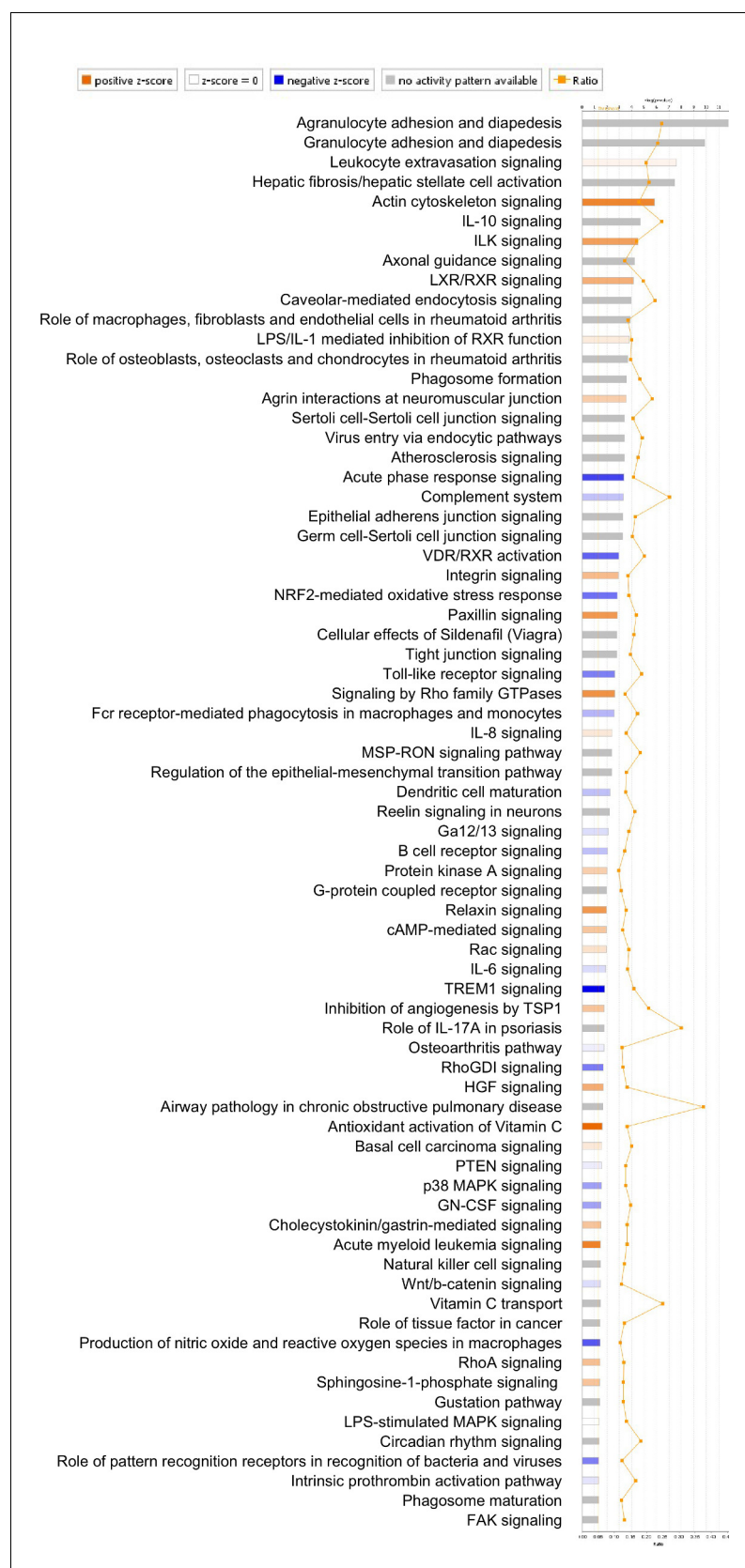


Figure 4—figure supplement 1. Pathway analysis of differentially expressed genes identified in RNA-Seq analysis of control and *Vangl2^{fl/fl}; Sox9^{Cre/+}* lungs at postnatal (P) day 5. p-value and z-score were shown. The calculated z-score is shown in the legend. *Figure 4—figure supplement 1 continued on next page*

Figure 4—figure supplement 1 continued

score indicates the prediction of overall increase or decrease in pathway activity. For a z-score >0 , the pathway is expected to be activated; for a z-score <0 , the pathway is expected to be inhibited. The ratio indicates the ratio of genes from the dataset that map to the pathway divided by the total number of genes that map to the same pathway. The orange line indicates a threshold of $-\log(\text{p-value}) = 1.30$ ($p < 0.05$) and the cutoff was set at $-\log(\text{p-value}) = 3$ ($p < 0.001$).

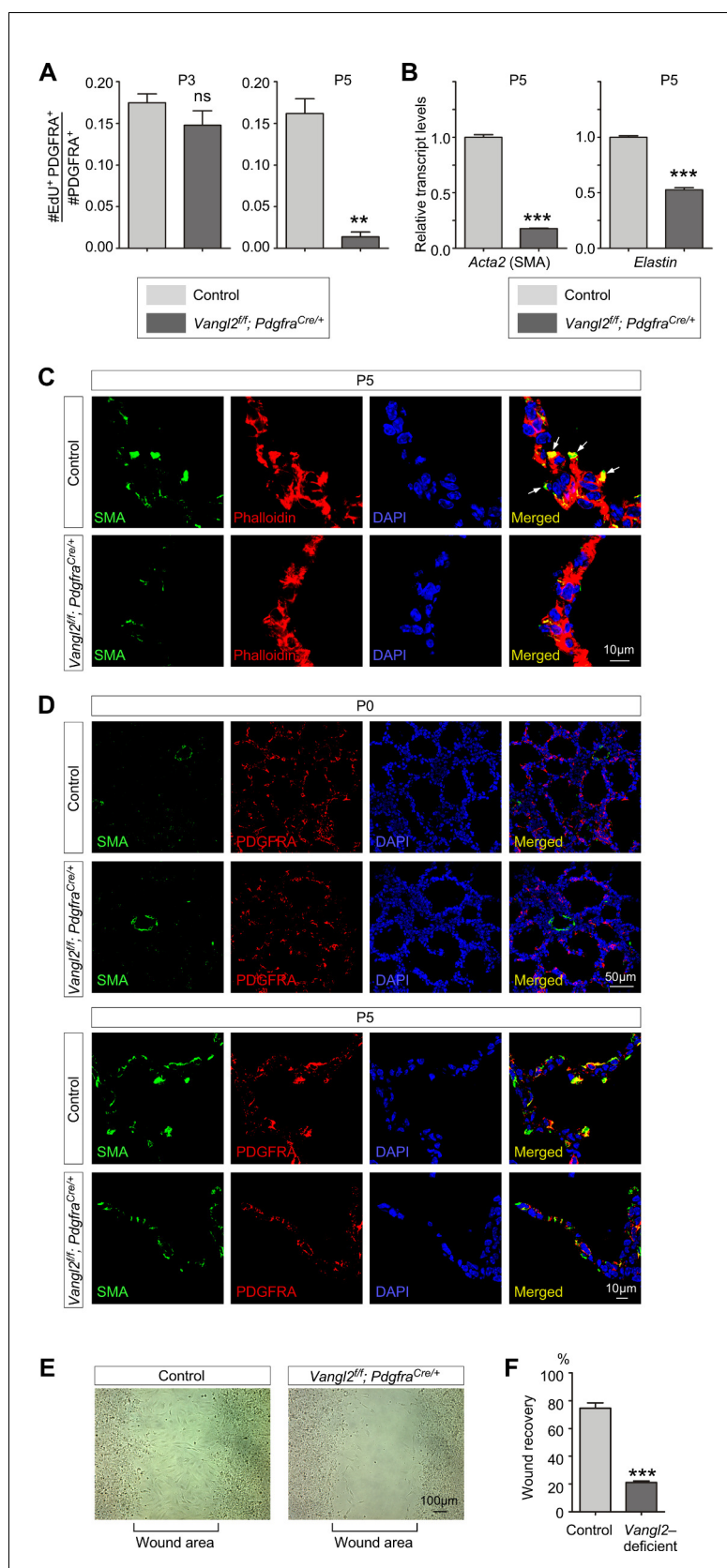


Figure 5. *Vangl2* regulates the cytoskeleton of myofibroblasts and their migration. (A) Quantification of myofibroblast proliferation in control and *Vangl2^{fl/fl}; Pdgfra^{Cre/+}* lungs at postnatal (P) day 3 and 5. The rate of

Figure 5 continued on next page

Figure 5 continued

myofibroblast proliferation was calculated as the ratio of the number of EdU⁺ myofibroblasts (EdU⁺PDGFRA⁺) to the number of myofibroblasts (PDGFRA⁺). An apparent reduction in the percentage of proliferating myofibroblasts was detected in *Vangl2^{fl/fl}; Pdgfra^{Cre/+}* lungs compared to controls ($n = 3$ for each group) at P5 but not at P3. (B) qPCR analysis of *Acta2* (SMA) and *Elastin* in control and *Vangl2^{fl/fl}; Pdgfra^{Cre/+}* lungs at P5. The mRNA levels of *Acta2* and *Elastin* were significantly reduced in the absence of *Vangl2* in myofibroblasts ($n = 3$ for each group). (C) Immunostaining of lung sections collected from control and *Vangl2^{fl/fl}; Pdgfra^{Cre/+}* mice at P5. The actomyosin cytoskeleton (stained by phalloidin) failed to organize around the prospective sites of secondary septa formation in *Vangl2^{fl/fl}; Pdgfra^{Cre/+}* lungs. In addition, smooth muscle actin (SMA) levels were significantly reduced and did not form stress fibers at the prospective sites of secondary septation. Arrows point to rudimentary secondary septa in control lungs. (D) Immunostaining of lung sections collected from control and *Vangl2^{fl/fl}; Pdgfra^{Cre/+}* mice at P0 and P5. Migration of myofibroblasts (PDGFRA⁺/SMA⁺) to the prospective sites of secondary septa failed to occur in the mutant lungs. (E) Wound recovery assays to assess the migratory ability of myofibroblasts derived from control and *Vangl2^{fl/fl}; Pdgfra^{Cre/+}* lungs. Within 36–48 hr, the wound area has been populated by migrating myofibroblasts derived from control lungs. By contrast, few myofibroblasts from *Vangl2^{fl/fl}; Pdgfra^{Cre/+}* lungs reached the wound area within the same time frame. (F) Quantification of wound recovery by myofibroblasts derived from control and *Vangl2^{fl/fl}; Pdgfra^{Cre/+}* lungs within 36–48 hr ($n = 3$ for each group). These results imply that mesenchymal *Vangl2* controls subsequent myofibroblast proliferation after the initial expansion or the migration defect exerts a secondary effect on myofibroblast proliferation or both. All values are mean \pm SEM. (***) $p < 0.001$ (unpaired Student's *t*-test).

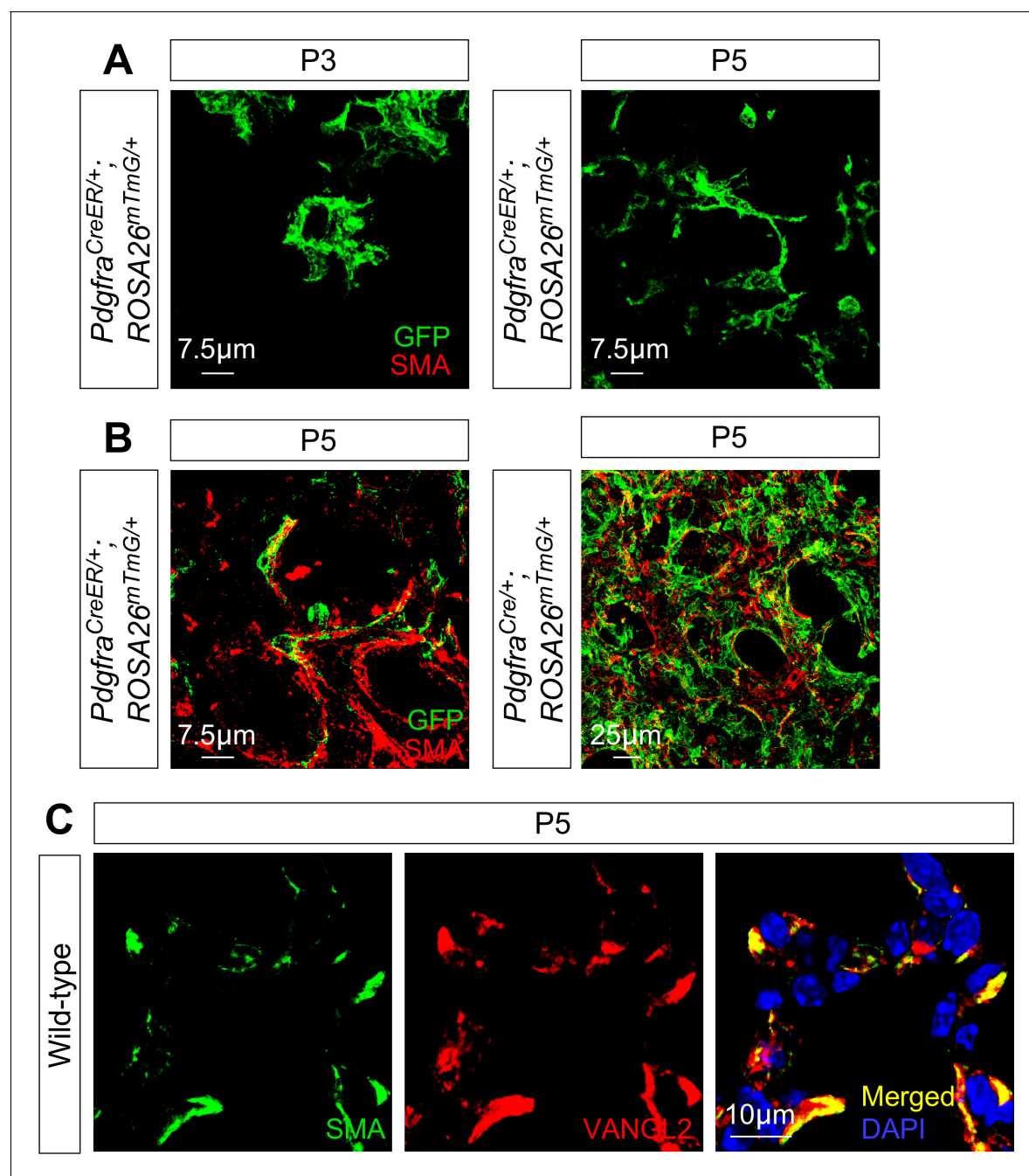


Figure 5—figure supplement 1. Myofibroblasts send out cellular extensions to form a network during alveologenesis. (A) Immunostaining of lung sections from *Pdgfra*^{CreER/+}; *ROSA26*^{mTmG/+} mice at postnatal (P) day 3 and 5. Leaky CreER expression labeled myofibroblasts. Cellular extensions of myofibroblasts became apparent at P5. (B) Immunostaining of lung sections from *Pdgfra*^{CreER/+}; *ROSA26*^{mTmG/+} or *Pdgfra*^{Cre/+}; *ROSA26*^{mTmG/+} mice at P5. Confocal stacks were shown to visualize the network of myofibroblasts. Smooth muscle actin (SMA) localized to cellular extensions of myofibroblasts. (C) Immunostaining of lung sections from wild-type mice at P5. VANGL2 and SMA colocalized at the cellular extensions of myofibroblasts.

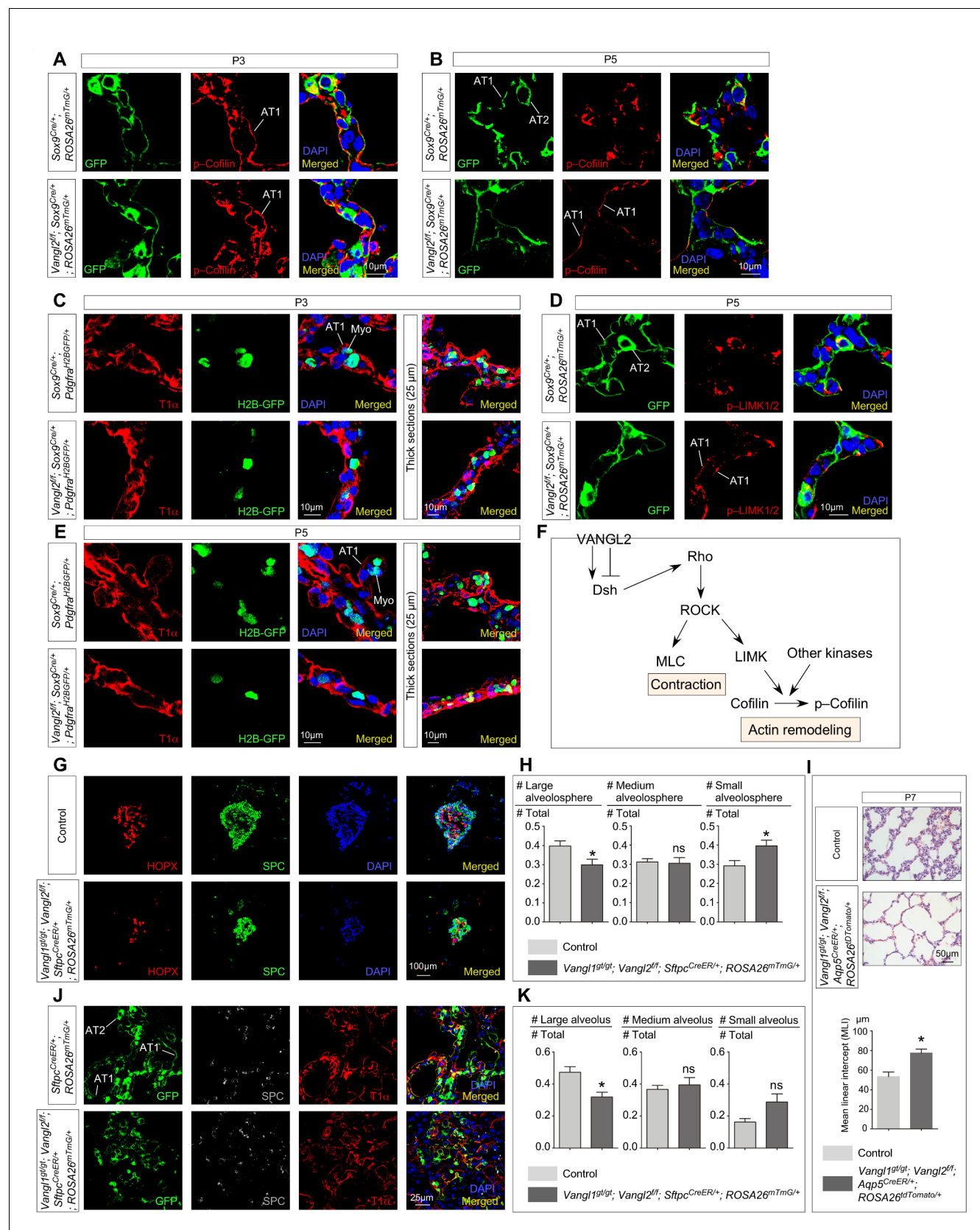


Figure 6. *Vangl2* controls the cytoskeleton of alveolar type I cells, their cell shape changes and their ability in forming alveolospheres and new alveoli. (A, B, D) Immunostaining of lung sections collected from *Sox9^{Cre/+}; ROSA26^{mTmG/+}* (control) and *Vangl2^{fl/fl}; Sox9^{Cre/+}; ROSA26^{mTmG/+}* mice at postnatal Figure 6 continued on next page

Figure 6 continued

(P) day 3 and 5. GFP from the *ROSA26* locus (*ROSA26^{mTmG}*) was activated in both alveolar type I (AT1) and type II (AT2) cells which could be distinguished by their morphology. The levels of phosphorylated (p) Cofilin and LIMK were significantly reduced in AT1 cells in control lungs by P5. By contrast, p-Cofilin and p-LIMK persisted in AT1 cells in *Vangl2^{f/f}; Sox9^{Cre/+}; ROSA26^{mTmG/+}* lungs. (C, E) Immunostaining of lung sections collected from *Sox9^{Cre/+}; Pdgfra^{H2BGFP/+}* (control) and *Vangl2^{f/f}; Sox9^{Cre/+}; Pdgfra^{H2BGFP/+}* mice at P3 and P5. Cell shape change of AT1 cells (T1 α ⁺) was observed in control lungs at the prospective sites of secondary septation to encase myofibroblasts (H2BGFP⁺) (myo) that had migrated toward AT1 cells. AT1 cells in *Vangl2^{f/f}; Sox9^{Cre/+}; Pdgfra^{H2BGFP/+}* lungs failed to undergo similar morphological changes. (F) Schematic diagram of a *Vangl2*-initiated signaling cascade that leads to phosphorylation of Cofilin and actin remodeling. (G) Immunostaining of alveolospheres derived from control and *Vangl1^{gt/gt}; Vangl2^{f/f}; Sftpc^{CreER/+}; ROSA26^{mTmG/+}* mice injected with tamoxifen. Both SPC⁺ and HOPX⁺ cells were found in alveolospheres derived from control and *Vangl1^{gt/gt}; Vangl2^{f/f}; Sftpc^{CreER/+}; ROSA26^{mTmG/+}* mice despite a difference in size and organization. (H) Quantification of the percentage of large (cross-sectional area >0.06mm²), medium (cross-sectional area between 0.015mm² and 0.06mm²) and small (cross-sectional area <0.015mm²) alveolospheres derived from control and *Vangl1^{gt/gt}; Vangl2^{f/f}; Sftpc^{CreER/+}; ROSA26^{mTmG/+}* mice (n = 5 for each group). The percentage of large alveolospheres derived from *Vangl1^{gt/gt}; Vangl2^{f/f}; Sftpc^{CreER/+}; ROSA26^{mTmG/+}* mice was reduced. (I) Hematoxylin and eosin-stained lung sections of wild-type and *Vangl1^{gt/gt}; Vangl2^{f/f}; Aqp5^{CreER/+}; ROSA26^{tdTomato/+}* mice injected with tamoxifen and collected at P7. Enlarged saccules were found in *Vangl1^{gt/gt}; Vangl2^{f/f}; Aqp5^{CreER/+}; ROSA26^{tdTomato/+}* lungs with an increased MLI in comparison with controls (n = 3 for each group). (J) Immunostaining of lung sections collected from *Sftpc^{CreER/+}; ROSA26^{mTmG/+}* (control) and *Vangl1^{gt/gt}; Vangl2^{f/f}; Sftpc^{CreER/+}; ROSA26^{mTmG/+}* mice injected with tamoxifen and treated with bleomycin. Lungs were harvested at 30 days post-bleomycin administration. In control lungs, GFP-labeled AT2 cells proliferated and differentiated into AT1 cells to form new alveoli. By contrast, fewer alveoli were produced in *Vangl1^{gt/gt}; Vangl2^{f/f}; Sftpc^{CreER/+}; ROSA26^{mTmG/+}* lungs. (K) Quantification of the percentage of large (cross-sectional area >0.6mm²), medium (cross-sectional area between 0.2mm² and 0.6mm²) and small (cross-sectional area <0.2mm²) alveoli derived from *Sftpc^{CreER/+}; ROSA26^{mTmG/+}* (control) and *Vangl1^{gt/gt}; Vangl2^{f/f}; Sftpc^{CreER/+}; ROSA26^{mTmG/+}* mice (n = 5 for each group). The percentage of large alveoli in *Vangl1^{gt/gt}; Vangl2^{f/f}; Sftpc^{CreER/+}; ROSA26^{mTmG/+}* lungs was reduced. All values are mean \pm SEM. (*) p<0.05; (**) p<0.01; (***) p<0.001; ns, not significant (unpaired Student's t-test).

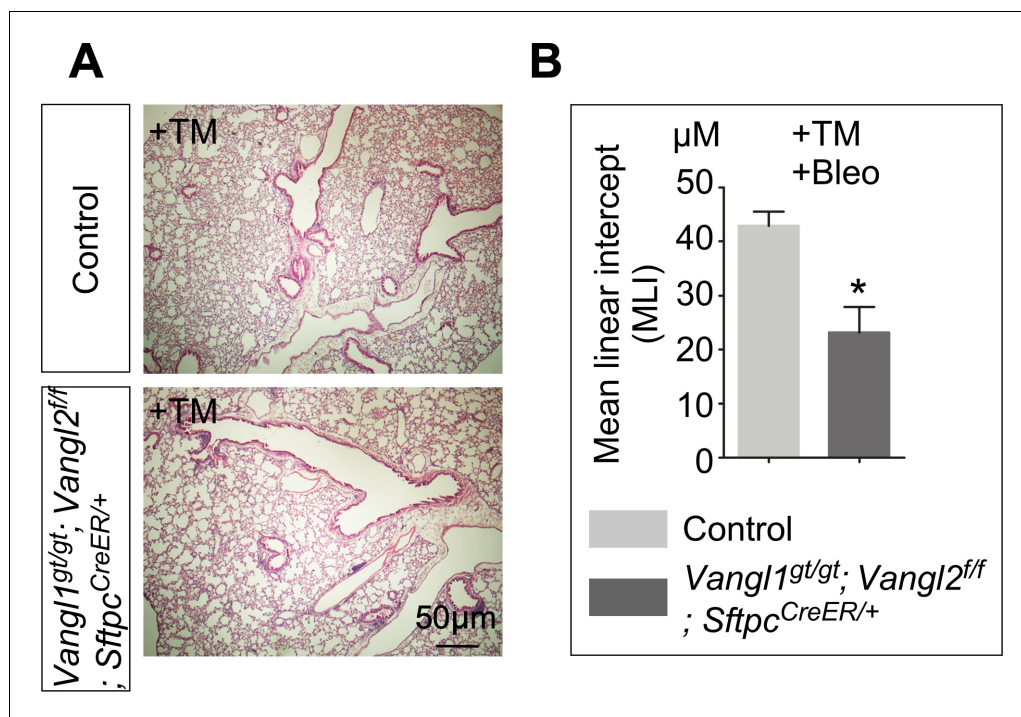


Figure 6—figure supplement 1. Bleomycin-induced lung injury results in a reduced MLI in the absence of *Vangl1/2*. (A) Hematoxylin and eosin-stained lung sections of control and *Vangl1^{gt/gt}; Vangl2^{f/f}; Sftpc^{CreER/+}* mice, which received tamoxifen (TM) injection. Lungs collected at 3 months post-TM (without bleomycin treatment) showed no evidence of lung fibrosis. (B) Measurement of the mean linear intercept (MLI) in control and *Vangl1^{gt/gt}; Vangl2^{f/f}; Sftpc^{CreER/+}* mice, which received TM and subsequently bleomycin. Lungs collected at one month post-bleomycin showed a reduction in the MLI of the mutant lungs. The reduced MLI in *Vangl1^{gt/gt}; Vangl2^{f/f}; Sftpc^{CreER/+}* lungs indicates a reduced distance between two primary or secondary septa in the regenerating alveoli, consistent with the definition of smaller alveoli. Smaller alveoli may be related to alterations in the cytoskeleton in the absence of *Vangl1/2*. All values are mean SEM. (*) $p < 0.05$ (unpaired Student's *t*-test).

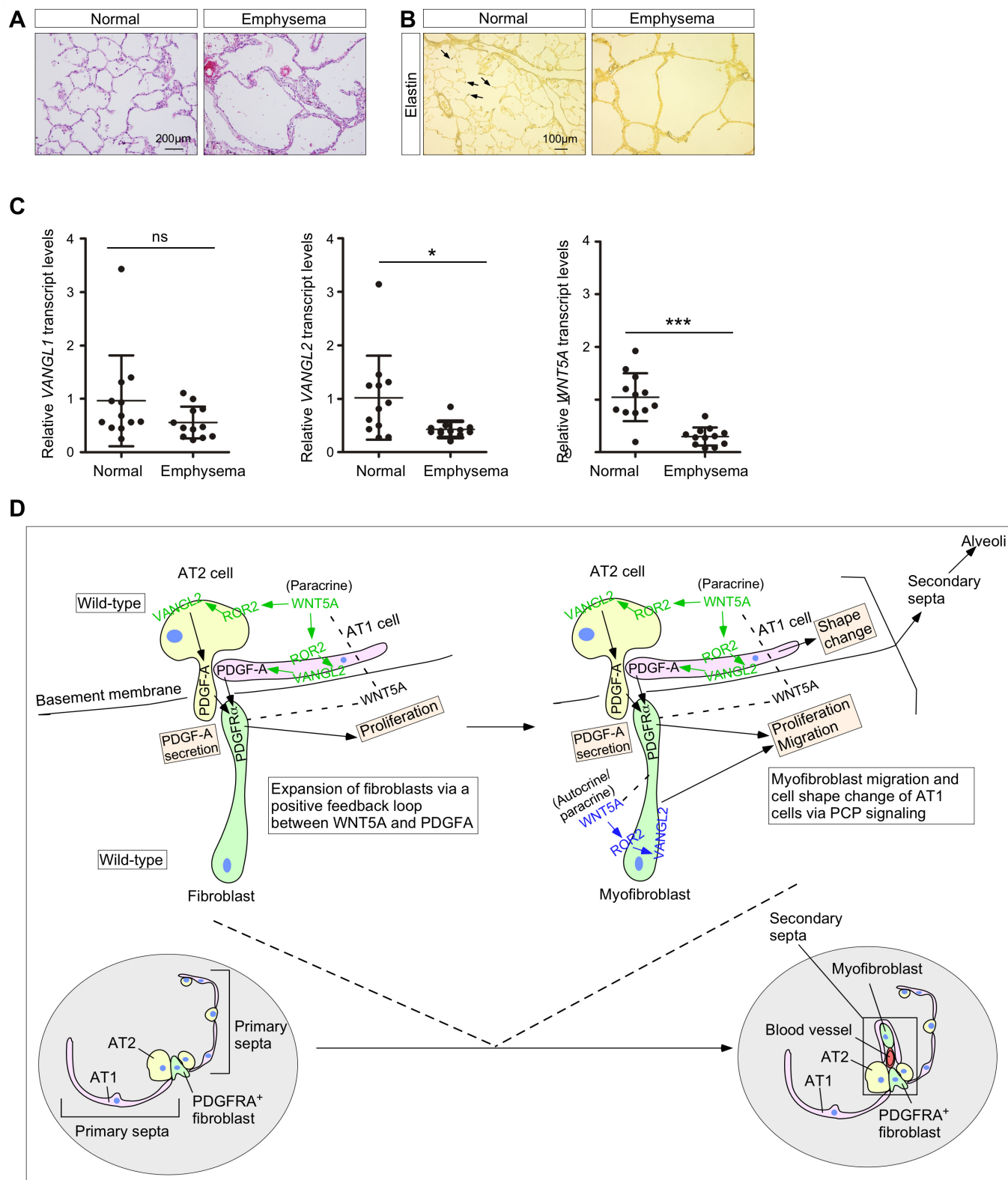


Figure 7. The WNT–VANG axis is downregulated in the lungs of human emphysema patients. (A) Hematoxylin and eosin-stained lung sections of normal and emphysema patients. Characteristic disruption of alveoli was observed in emphysema patients, resulting in increased airspace. (B) Elastin

Figure 7 continued on next page

Figure 7 continued

staining of lung sections of normal and emphysema patients. The slides were counterstained with tartrazine. Elastin, which was detected at the secondary septa in normal lungs (arrows), was greatly reduced in the lungs of emphysema patients. (C) qPCR analysis of *VANGL1*, *VANGL2* and *WNT5A* in lungs from normal and emphysema patients ($n = 12$ for each group). The mRNA levels of *VANGL2* and *WNT5A* were significantly reduced in emphysema patients. All values are mean \pm SEM. (*) $p < 0.05$; (**) $p < 0.01$; (***) $p < 0.001$; ns, not significant (unpaired Student's *t*-test). (D) A new model of alveolar formation through control of cellular properties by PCP signaling. We propose that epithelial PCP signaling via the *Wnt5a–Ror2–Vangl2* axis (colored green) controls PDGF secretion from alveolar type I and type II cells to promote proliferation of mesenchymal fibroblasts. In this process, a positive feedback loop between *WNT5A* and PDGF leads to expansion of the fibroblast pool required for subsequent alveologenesis. The expanded fibroblast population expresses SMA and becomes myofibroblasts, which continue to proliferate. In addition, myofibroblasts migrate to the prospective site of secondary septation in response to PCP signaling (colored blue). Likewise, epithelial PCP signaling (colored green) instructs cell shape changes of alveolar type I cells necessary for encasing myofibroblasts that migrate toward the site of secondary septation. All of these cellular events (orange-colored boxes) are due to modulation of the actomyosin cytoskeleton via the *Wnt5a–Ror2–Vangl2* axis.